

Optical follow-up of gravitational wave events during the second advanced LIGO/VIRGO observing run with the DLT40 Survey

SHENG YANG,^{1,2,3} DAVID J. SAND,⁴ STEFANO VALENTI,¹ ENRICO CAPPELLARO,³ LEONARDO TARTAGLIA,^{5,4}
 SAMUEL WYATT,⁴ ALESSANDRA CORSI,⁶ DANIEL E. REICHART,⁷ JOSHUA HAISLIP,⁷ AND VLADIMIR KOUPRIANOV^{7,8}
 (DLT40 COLLABORATION)

¹Department of Physics, University of California, 1 Shields Avenue, Davis, CA 95616-5270, USA

²Department of Physics and Astronomy Galileo Galilei, University of Padova, Vicolo dell’Osservatorio, 3, I-35122 Padova, Italy

³INAF Osservatorio Astronomico di Padova, Vicolo dell’Osservatorio 5, I-35122 Padova, Italy

⁴Department of Astronomy/Steward Observatory, 933 North Cherry Avenue, Room N204, Tucson, AZ 85721-0065, USA

⁵Department of Astronomy and The Oskar Klein Centre, AlbaNova University Center, Stockholm University, SE-106 91 Stockholm, Sweden

⁶Physics & Astronomy Department, Texas Tech University, Lubbock, TX 79409, USA

⁷Department of Physics and Astronomy, University of North Carolina at Chapel Hill, Chapel Hill, NC 27599, USA

⁸Central (Pulkovo) Observatory of Russian Academy of Sciences, 196140 Pulkovskoye Ave. 65/1, Saint Petersburg, Russia

(Received XXX; Revised YYY; Accepted ZZZ)

Submitted to ApJ

ABSTRACT

We describe the gravitational wave (GW) follow-up strategy and subsequent results of the Distance Less Than 40 Mpc survey (DLT40) during the second science run (O2) of the Laser Interferometer Gravitational-wave Observatory and Virgo collaboration (LVC). Depending on the information provided in the GW alert together with the localization map sent by the LVC, DLT40 would respond promptly to image the corresponding galaxies selected by our ranking algorithm in order to search for possible electromagnetic (EM) counterparts in real time. During the LVC O2 run, DLT40 followed ten GW triggers, observing between \sim 20-100 galaxies within the GW localization area of each event. From this campaign, we identified two real transient sources within the GW localizations with an appropriate on-source time – one was an unrelated type Ia supernova (SN 2017cbv), and the other was the optical kilonova, AT 2017fg0/SSS17a/DLT17ck, associated with the binary neutron star coalescence GW170817 (a.k.a gamma-ray burst GRB170817A). We conclude with a discussion of the DLT40 survey’s plans for the upcoming LVC O3 run, which include expanding our galaxy search fields out to $D \approx 65$ Mpc to match the LVC’s planned three-detector sensitivity for binary neutron star mergers.

Keywords: gravitational wave: general — gravitational wave: individual (GW170104, GW170608, GW170809, GW170814, GW170817, GW170823) — methods:observational

1. INTRODUCTION

The long-awaited direct detection of gravitational waves (GWs) by first the Advanced Laser Interferometer Gravitational-wave Observatory (LIGO; [Aasi et al. 2015](#)) and then the Advanced Virgo interferometer ([Acernese et al. 2015](#)) has ushered in a new era of physics. These exquisite detectors are designed to probe high

frequency (\sim 10–1000 Hz) GW signals whose main astrophysical sources are compact binary coalescences (CBCs) – i.e. binary black hole (BBH), black hole – neutron star and binary neutron star (BNS) mergers.

During the first Advanced LIGO observing run (O1), two BBH GW events were detected (GW150914; [Abbott et al. 2016e](#), and GW151226; [Abbott et al. 2016b](#)), along with a third likely event of astrophysical origin (LVT151012; [Abbott et al. 2016a](#)). While BBH mergers are not generally expected to have electro-

Corresponding author: Sheng Yang
sheng.yang@inaf.it

magnetic (EM) counterparts¹, the astronomical community (joined by neutrino and cosmic-ray researchers) promptly responded and searched for transients associated with these BBH events (see e.g. Abbott et al. 2016c, for a summary of the follow-up of GW150914), partly in preparation for GW events which are expected to have an EM counterpart, namely those with a neutron star as one of the constituents.

The participation of the EM, neutrino and cosmic ray communities continued in the second LVC observing season (O2), with hundreds of telescopes and detectors participating in the follow-up of GW sources. During O2, the Advanced LIGO detectors were significantly more sensitive, and were joined by Virgo in the final month of data taking – this is significant, as the addition of a third detector can decrease the GW localization regions from $\sim 100\text{-}1000 \text{ deg}^2$ to $\sim 10\text{-}100 \text{ deg}^2$ for high signal-to-noise events (Abbott et al. 2018). In total, fourteen GW alerts were issued by the LVC, six of which were ultimately determined to be true GW events (The LIGO Scientific Collaboration & the Virgo Collaboration 2019). Many of these were aggressively pursued by the astronomical community, whose efforts finally bore fruit with the GW170817 BNS merger (Abbott et al. 2017c), which led to the discovery of the first EM counterpart of a GW event (from gamma-ray to radio wavelengths; Abbott et al. 2017d; Coulter et al. 2017; Valenti et al. 2017; Tanvir et al. 2017; Lipunov et al. 2017; Soares-Santos et al. 2017a; Arcavi et al. 2017a; Goldstein et al. 2017; Savchenko et al. 2017; Haggard et al. 2017; Troja et al. 2017; Hallinan et al. 2017; Margutti et al. 2017).

In this paper we describe the observational campaign performed by the Distance Less Than 40 Mpc (DLT40) project and its GW follow-up efforts during the LVC O2 run. Elsewhere we have described the co-discovery of AT2017gfo/SSS17a/DLT17ck and the DLT40 team’s follow-up observations (Valenti et al. 2017) and the limit to the Kilonova rate using the DLT40 search (Yang et al. 2017). In Section 2 we provide an overview of the DLT40 supernova and transient program. A description of the DLT40 GW follow-up strategy in particular is described in Section 3. Next, in Section 4 we present the results of the DLT40 follow-up during O2. We discuss the DLT40 program’s specific upgrades and plans for the imminent

¹ Whether a BBH merger can produce an EM signal is still an open question. A weak gamma-ray transient was reported 0.4 s after GW150914, consistent with the GW localization (Connaughton et al. 2016). Subsequent models and theoretical work (Loeb 2016; Perna et al. 2016, 2018; Zhang et al. 2016; Bartos et al. 2017; de Mink & King 2017) make the continued search for EM counterparts to BBHs a source of interest.

O3 observing run in Section 5. We end the paper with a brief discussion and summary (Section 6).

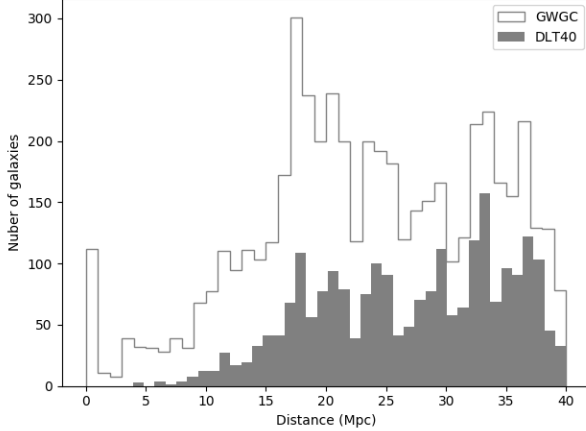
2. DLT40 TRANSIENT SEARCH

The DLT40 survey is designed as a high cadence supernova search. By targeting luminous galaxies within $D < 40 \text{ Mpc}$, we aim to find ~ 10 supernovae per year within ~ 1 day of explosion. More details of the program are presented elsewhere (Tartaglia et al. 2018; Yang et al. 2017) which we generally summarize here. During the Advanced Detector O2 run, DLT40 used a PROMPT 0.4m telescope (PROMPT5; Reichart et al. 2005) which has a field of view (FoV) of $10 \times 10 \text{ arcmin}^2$ and is located at Cerro Tololo Inter-American Observatory (CTIO), part of the Skynet Robotic Telescope Network ². In a typical night, $\sim 400\text{-}500$ galaxies are observed. The exposure time per field is 45 s, and the data is taken with no filter, yielding a typical limiting magnitude of $r \sim 19$ mag. The DLT40 galaxy sample is selected from the Gravitational Wave Galaxy Catalogue (GWGC; White et al. 2011), with further cuts made on recessional velocity ($V < 3000 \text{ km s}^{-1}$ which corresponds to $D \lesssim 40 \text{ Mpc}$), declination ($\text{Dec} < +20 \text{ deg}$), absolute magnitude ($M_B < -18 \text{ mag}$), and Milky Way extinction ($A_V < 0.5 \text{ mag}$). We maintained our original DLT40 galaxy sample even after the Galaxy List for the Advanced Detector Era (GLADE³) was made available because the completeness of the two catalogues is not significantly different within 40 Mpc (Dálya et al. 2018). The physical properties of the ~ 2200 galaxies in the DLT40 sample are shown in Figure 1 in comparison to the whole GWGC sample within $D < 40 \text{ Mpc}$, selected without a luminosity cut.

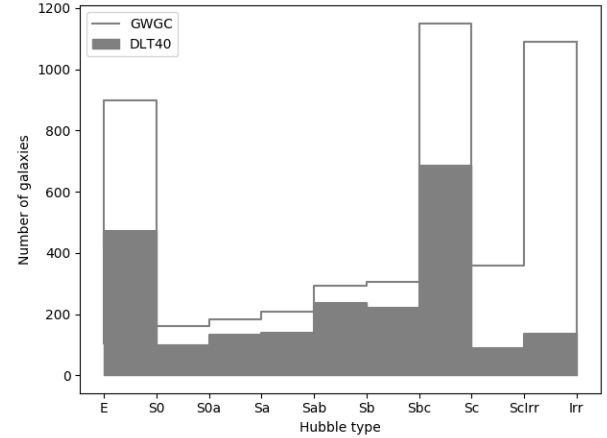
The DLT40 survey is fully robotic, and a flowchart of operations is shown in Figure 2. A schedule is submitted automatically every afternoon before the Chilean sunset, and targets are given a priority between one and five. A score of five is the highest priority, and is reserved only for the most important targets such as the galaxies selected for GW follow-up. A score of four is assigned to galaxies that have been observed by the DLT40 survey over the last three days in order to maintain the program’s cadence. A select few other galaxies are also given a native score of four – for instance, if they are within $D < 11 \text{ Mpc}$, or if one PROMPT field of view can capture more than one DLT40 galaxy. A score of three is assigned to other DLT40 galaxies not selected with higher priority, and which have $M_B < -20 \text{ mag}$, while a score of two is assigned to those galaxies with $M_B < -19$

² <https://skynet.unc.edu/>

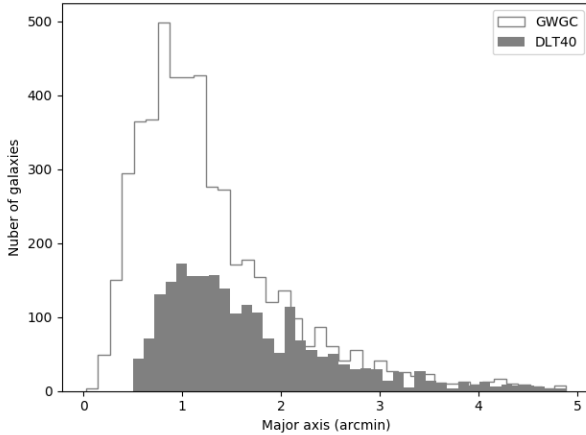
³ <http://aquarius.elte.hu/glade>



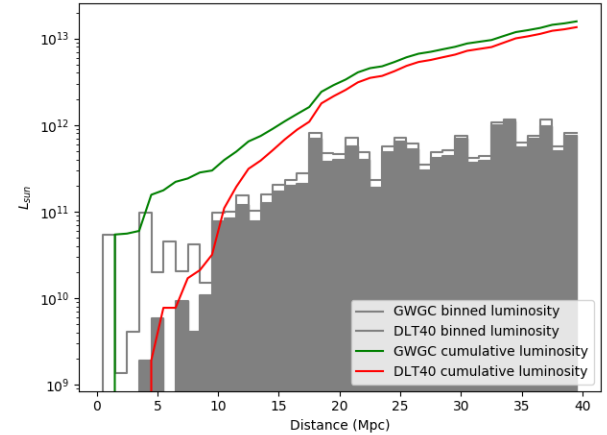
(a) The distance distribution of DLT40 (filled histogram) and GWGC galaxies within 40 Mpc (shaded histogram).



(b) The Hubble type distribution for DLT40 (shaded histogram) and GWGC galaxies (open histogram) within 40 Mpc.



(c) The major axis distribution (in arcmin) for DLT40 (shaded histogram) and GWGC galaxies within 40 Mpc (open histogram).



(d) The binned and integrated B band luminosity distribution for DLT40 and GWGC galaxies within 40 Mpc; note the binned points are difficult to distinguish on the scale of this plot.

Figure 1. Physical properties of the DLT40 galaxy sample compared with the GWGC (White et al. 2011).

mag. The remaining galaxies are given a score of one. The Skynet scheduler observes targets from west to east within a priority category so that all of the priority five galaxies are observed first (if visible), followed by the priority four galaxies, and so on. Galaxy priorities can not be assigned in a ‘fine-grained’ way beyond that described above, and so in this sense all of the galaxies targeted for the DLT40 GW search were observed with an equally high priority, observed from west to east.

After an exposure is completed, the Skynet Robotic Telescope Network system automatically detrends the data (i.e. applies bias and flat field corrections), and determines an astrometric world coordinate system solution before the image is ingested by the DLT40 pipeline. From there, image subtraction is performed with respect to a high quality template image using the publicly

available **Hotpants** code (Becker 2015). **SExtractor**⁴ (Bertin & Arnouts 1996) is then used to extract all sources in the difference images above a signal to noise threshold of five. The difference image source catalog typically includes a large number of spurious objects due to stochastic processes, small misalignments between the images, improper flux scalings, imperfect PSF matching between the template and target image, and cosmic rays. In order to filter out spurious candidates, a scoring algorithm was developed based on catalog parameters returned by **SExtractor**. This approach still required visual screening of a significant number of candidates, most of which are rejected. Recently we have imple-

⁴ <http://www.astromatic.net/software/sextractor>

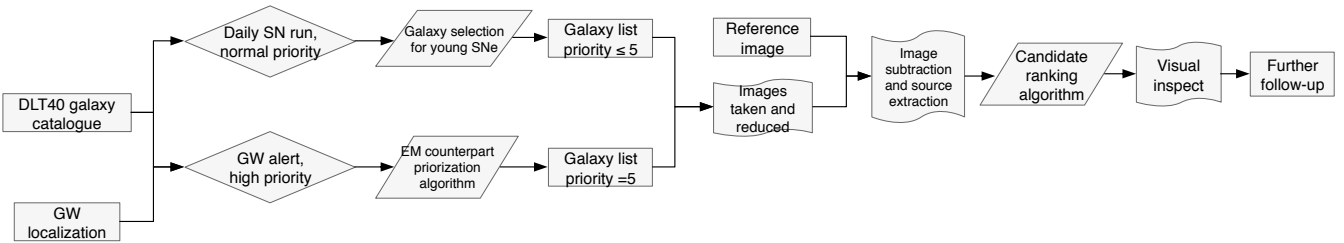


Figure 2. Work flowchart for the DLT40 survey.

mented a machine learning algorithm for better filtering the spurious objects, which we discuss briefly along with our plans for the third observing run of the Advanced Detectors in Section 5.2. In order to manage our real time data stream we use a MySQL⁵ database and visually inspect SN candidates through web pages powered by the Flask⁶ tool. After eyeballing, we secure immediate follow-up photometry or spectroscopy from collaborating facilities, most notably Las Cumbres Observatory, which itself is operated robotically (Brown et al. 2013).

The real time and quick response of the DLT40 SN search make it ideal for rapidly evolving transients including the EM counterparts to GW sources. As such, DLT40 joined the global search effort during the Advanced Detector O2 run. We discuss our GW follow-up strategy in more detail next.

3. GW FOLLOW-UP STRATEGY

The localization regions for GW events are still formidably large (especially compared to the DLT40 FoV), being of order $\lesssim 1000 \text{ deg}^2$ for two detector events and $\sim 10\text{-}100 \text{ deg}^2$ for three (e.g. Abbott et al. 2016d). Two complementary EM search strategies have been implemented by various groups thus far. The first involves direct tiling of the GW localization with wide-field telescopes in the search for counterparts (e.g. Smartt et al. 2016; Kasliwal et al. 2016; Abbott et al. 2016d; Soares-Santos et al. 2017b; Doctor et al. 2018, among others), while the second relies on a targeted galaxy search focused on systems at a distance consistent with the GW signal that are also within the localization region (e.g. Gehrels et al. 2016). The DLT40 program followed the galaxy-targeted approach, although we relaxed any distance constraints whenever a GW event was beyond the nominal ~ 40 Mpc horizon of the main SN search, as we describe below. The DLT40 PROMPT5 telescope’s field of view ($10'\times 10'$) corresponds to 20 kpc (40 kpc) at a distances of 20 Mpc (40 Mpc), which encompasses

$>90\%$ of expected merger-host offsets (Fong & Berger 2013), and so each galaxy can be targeted with a single pointing.

3.1. Galaxy prioritization

The DLT40 software suite ingests the GCN alerts employed during O2 for disseminating GW event information, and we download the HEALPIX localization map with distance constraints (see Singer & Price 2016; Singer et al. 2016, for further information on the generation of these maps). From this GW-based data, we prioritize galaxies in the DLT40 catalog given the position, relative probability within the localization map, and the galaxy’s inferred mass. Again, we ignore any distance constraints from the GW signal in our galaxy prioritization algorithm (except for the nearby event GW170817). The target prioritization process is implemented as follows (see also Figure 3):

1. The DLT40 galaxy catalog is mapped with the HEALPIX tool, weighted by galaxy luminosity (we assume that the mass distribution follows the *B*-band luminosity), and smoothed with a Gaussian corresponding to each galaxy’s reported radius. This yields a luminosity distribution map of DLT40 galaxies, S_{lum} , which we normalize (N_{lum}):

$$N_{lum} = \frac{S_{lum}}{\sum S_{lum}} \quad (1)$$

2. The GW probability map from LVC is already normalized as S_{gw} .

3. We then take the product of the DLT40 galaxy map and the GW probability map,

$$C = S_{gw} \times N_{lum} \quad (2)$$

4. For each DLT40 galaxy i , we sum over all pixels in C inside the galaxy radius, which yields our prioritization,

$$s_i = \sum_j C_{ij} \quad (3)$$

where j is the HEALPIX pixel value inside the specific radius.

⁵ <https://www.mysql.com/>

⁶ <http://flask.pocoo.org/>

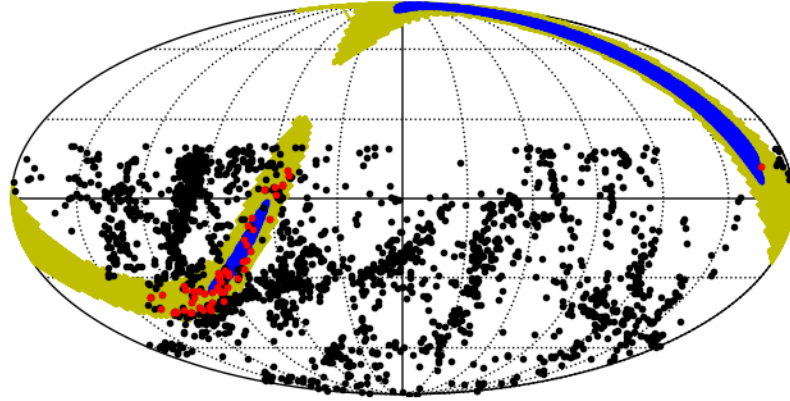


Figure 3. Illustration of the DLT40 galaxy ranking algorithm as applied to the LIGO trigger G275404. The full DLT40 galaxy sample is overlaid as black dots on the HEALPix GW probability map; the blue and yellow region presents the 68% and 95% GW confidence region, respectively. After normalization, a galaxy’s score is defined as the accumulated pixel values inside the galaxy area, convolved with the GW probability map. The top ranked galaxies are selected for immediate follow-up and monitoring as described in Section 3. In the case of G275404, the red dots show the selected galaxies – not all DLT40 galaxies within the LIGO 95% confidence region were observed. We observed up to a cumulative score of 0.99 (50 galaxies) in the initial phase of our follow-up (see Section 4.1).

After the galaxy prioritization procedure, a cut on the number of monitored galaxies was made based on the level of interest in the GW trigger and practical observing considerations. For some GW sources with very large localization regions, we would also make cuts based directly on these maps – for instance, only selecting galaxy targets within the 80% credible region; see Section 4 for details on individual sources. We would select galaxies by cutting the ranked list at the top 50% - 99% of the normalized cumulative score, s , which would then be further reduced since some galaxies in the list would be unobservable (i.e. below the horizon). For instance, if the GW trigger indicated the source was a local real (with a very low FAR) CBC, we would select galaxies up to a cumulative score of 99%, as shown in Figure 4. For those GW triggers that DLT40 followed up in O2, we observed between 18 and 114 galaxies per event, which corresponded to cumulative scores between 0.1 and 0.99. All the selected galaxies were set to priority 5 in the DLT40 scheduler.

As evidence of the efficacy of our galaxy prioritization algorithm, the highest priority galaxy for the binary neutron star event GW170817 was NGC 4993, the true host galaxy of the counterpart (see Section 4.2 and Table 13 for further details). We discuss each individual

GW event and our detailed follow-up from O2 further in Section 4.

In principle, we can adjust our galaxy prioritization to account for the GW-inferred distance (if given) and other detection efficiencies (similar to Arcavi et al. 2017b). For the LVC O2 run, we did not include the GW-inferred distance into our galaxy targeting algorithm (which were only available for CBC triggers), but will do so for the DLT40 O3 campaign (Section 5.2).

3.2. Monitoring timescale

The duration that we monitor GW-related galaxies depends on the type of trigger. For burst-type GW events that are possibly related to core-collapse supernovae (with an optical time scale of \sim 10-100 days), we adopt a monitoring period of three weeks. For binary neutron star-type mergers, an r-process kilonova (Li & Paczyński 1998; Metzger et al. 2010; Kasen et al. 2013) and/or short gamma-ray burst (sGRB) afterglow emission is expected. Figure 6 shows different light curve models for kilonovae and sGRB afterglow emission, scaled to a distance of 40 Mpc. As shown, DLT40 could detect transients predicted by most of the models out to this distance (the limiting magnitude of DLT40 is $r \sim 19$ mag, as measured by artificial star experiments, described in Yang et al. 2017). We thus conservatively

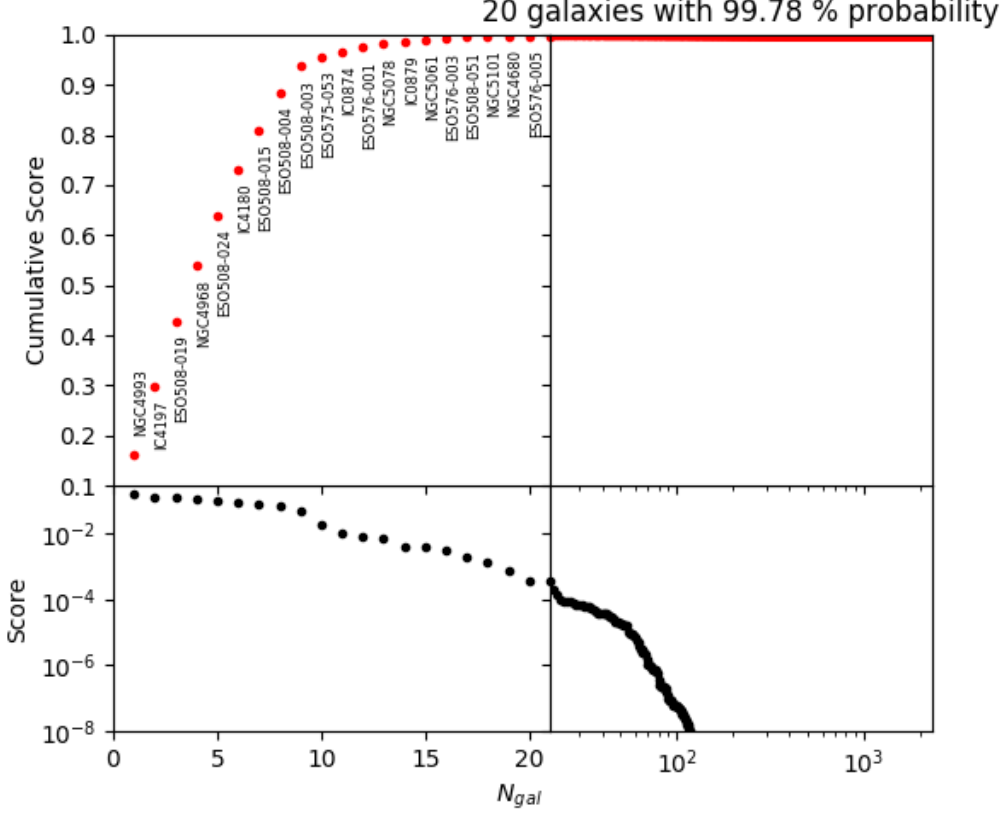


Figure 4. Cumulative score for DLT40 galaxies as prioritized for the NS-NS binary GW170817, using the algorithm described in Section 3. As shown, NGC 4993, the host of the kilonova DLT17ck/AT2017gfo, is ranked first. The twenty selected DLT40 galaxies cover 99.78% of the cumulative probability. More detailed information for each galaxy is presented in Table 13.

monitored compact binary events for ~ 2 weeks, well beyond the time we would generally expect to have a detection.

3.3. Summary

This galaxy prioritization process produces a list of galaxies that are sent automatically to the DLT40 scheduler. As discussed, these galaxies are observed at the highest priority, going from west to east on the sky, and are immediately ingested into our transient detection pipeline. All transient candidates were scored with our image feature-based algorithm and forwarded within minutes of data taking for visual inspection. If an interesting transient was found, a GCN was issued as soon as possible to facilitate follow-up observations; if no viable candidates were found, a summary GCN was usually posted in the following days to weeks.

4. SEARCH RESULTS IN O2

The LIGO O2 observing run ran from 2016 November 30 to 2017 August 25, with Virgo joining the network of GW detectors in early August, 2017. Fourteen GW alert triggers were issued (six of which turned out to be real events) by the LVC for follow-up to the EM community

(The LIGO Scientific Collaboration & the Virgo Collaboration 2019), among which we followed the ten triggers indicated in Table 1 with their localization shown in Figure 7. Three of these ten events that DLT40 followed up were ultimately found to be true GW events after further GW analysis (these are also marked in Table 1).

DLT40 pursued BBH events without prejudice during O2, even though these events may not have associated EM emission. GW horizon distances of BBH events are typically relatively large compared to the nominal reach of the DLT40 survey (focused on galaxies within 40 Mpc). For instance, the initial luminosity distance of G275697 estimated by the LVC has a mean value of 181 Mpc and standard deviation 55 Mpc (see Table 1; LIGO Scientific Collaboration & Virgo Collaboration 2017j). The cumulative probability within a 40 Mpc volume is only 1%. However, we activated our follow-up search for GW events outside the nominal DLT40 distance horizon for the following reasons:

- As mentioned, during the LVC O2 run, the distance estimates of CBC are generally available, but are sometimes updated later or not reported in early circulars.

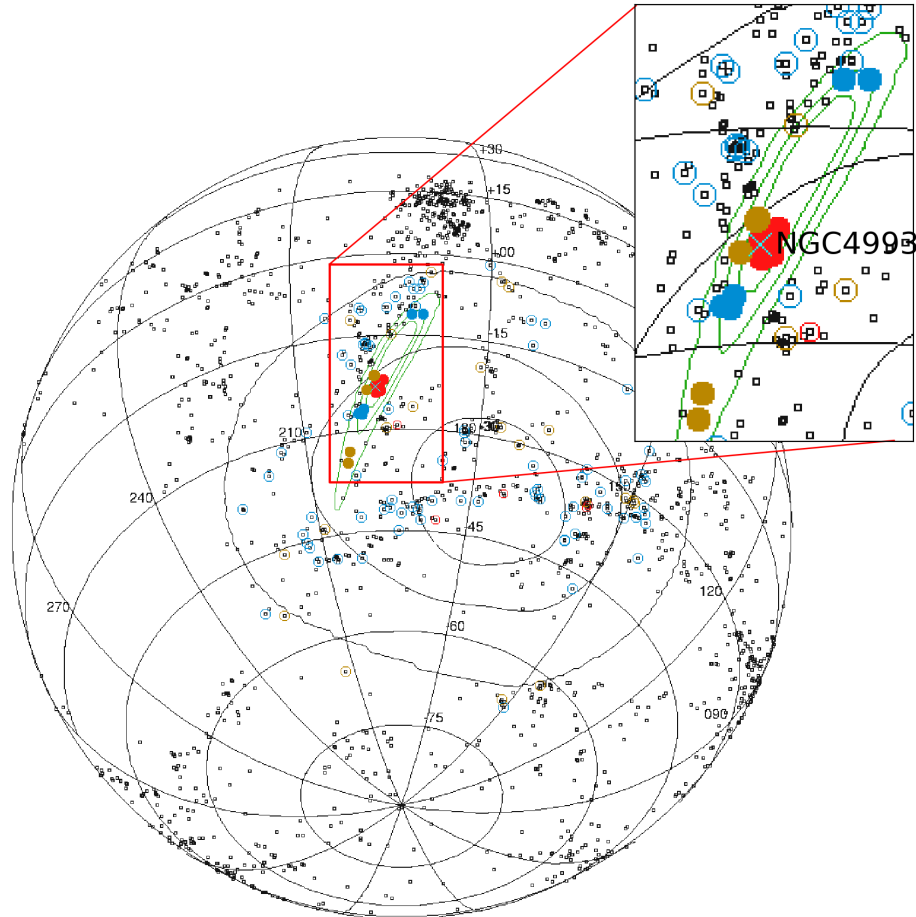


Figure 5. Localization region (contours) and the matched galaxies (circles) for GW170817/G298048 (solid circles) and GRB170817a (hollow circles). The contours indicate 50%, 90%, and 99% confidence bounds while the GW trigger is shown in green and the GRB trigger is shown in black. The colors of the circles denote the priority of the galaxies (high priority in red, normal priority in yellow and low priority in blue). All the DLT40 galaxy samples are shown as black dots. After ranking, we decided to follow all 20 GW galaxies (9 high + 5 normal + 6 low) and the top 31 GRB galaxies (5 high + 26 normal).

- DLT40 is not dedicated to GW follow-up, so there is no conflict with our daily SN search – it does not harm us to search even if the probability of success is low.
- The search could be implemented as a test run in preparation for events that DLT40 is more likely to find counterparts for (e.g. GW170817; Valenti et al. 2017).

For such BBH events with estimated GW distance beyond the reach of DLT40, we activated only the top 50% of galaxies scored by our ranking algorithm (see Section 3).

Here we present our observations for the ten DLT40-followed GW triggers, focusing first on the two events where our team identified optical transients. Unless otherwise noted, all dates listed are UTC. Detailed observational logs for each event are presented as a series of tables in the Appendix.

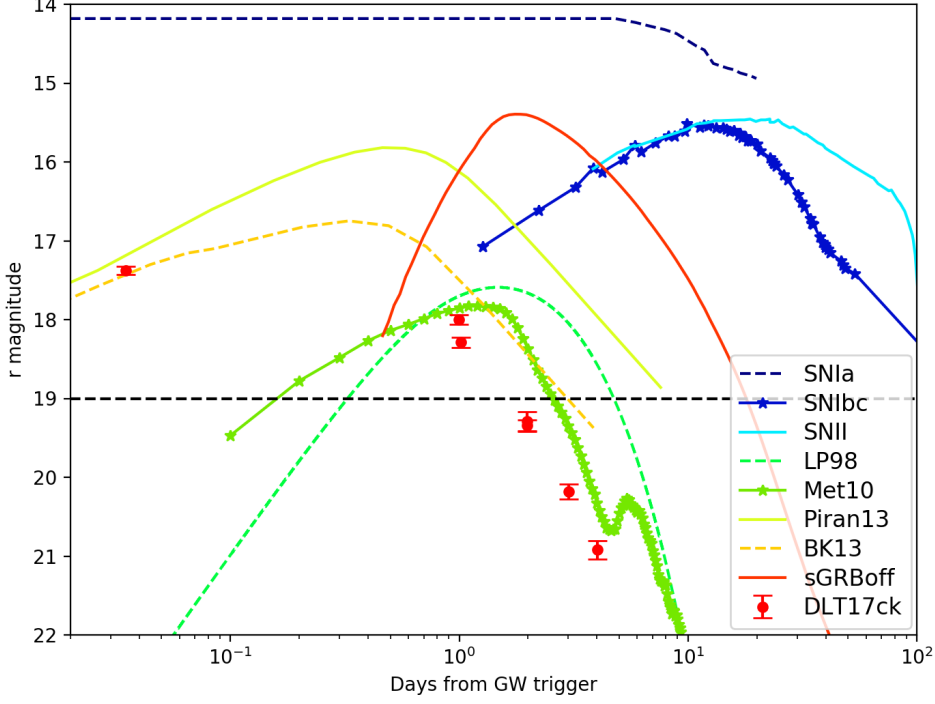


Figure 6. Several possible EM emission models of GW sources, scaled to a distance of 40 Mpc, are plotted against the 6 epochs of DLT17ck observations (red dots), as measured by the DLT40 survey (Valenti et al. 2017). Among these optical emission models, there are four kilonova models: LP98 (Li & Paczyński 1998), assuming a blackbody emission for an ejecta mass $10^{-2}M_{\odot}$, and outflow speed of $v = 0.1c$; Met10 (Metzger et al. 2010), assuming a radioactively powered emission with an ejecta mass $10^{-2}M_{\odot}$, and outflow speed of $v = 0.1c$, as well as iron-like opacities; BK13 (Barnes & Kasen 2013), assuming an ejected mass of $10^{-3}M_{\odot}$ and velocity of $0.1c$, along with lanthanide opacities; Piran13 (Piran et al. 2013), assuming a BH-NS merger with $NS = 1.4M_{\odot}$, $BH = 10M_{\odot}$. We also include one sGRB off axis model: sGRBoff (van Eerten & MacFadyen 2011), a simulated off-axis afterglow light curve assuming a short GRB with ejecta energy of $E_{jet} = 10^{50}erg$, interstellar matter density of $n = 10^{-3}cm^{-3}$, jet half-opening angle of $\theta_{jet} = 0.2$ radians and an observed viewing angle of $\theta_{obs} = 0.2$ radians. For comparison, we also show three SN light curves, including SN 2012cg (a type Ia SN; Marion et al. 2016), SN2002ap (a type Ib/c SN) and SN SN2013ej (a type II SN; Yuan et al. 2016).

Table 1. Summary table of DLT40 follow-up of LVC O2 triggers. GW alert properties include the source type, the false alarm rate (FAR), the 90% confidence level sky localization area, and the luminosity distance. In the second column block, we report DLT40 observations, including the number of galaxies observed, their observation window, possible transients detected by DLT40 in that dataset, and the reference GCNs. It should be mentioned that the GW estimates shown here are taken from the LVC preliminary and updated GCNs, the final GW estimation is shown in The LIGO Scientific Collaboration & the Virgo Collaboration (2019).

GW/GRB trigger	Source type	LVC GW estimations				DLT40 EM observations				REF ^e
		FAR ^a (yr ⁻¹)	Localization ^b (deg ²)	D _{lum} (Mpc)	ref ^c	N _{gal}	Obs_window (JD)	Detection ^d or r _{lim}		
GW170104 ^f (G268556)	CBC	2	1600	...	a	18	2457759- 2457766
G270580 ^f	Burst	5	3100	...	b c	25	2457774-	19.2	A	

Table 1 continued

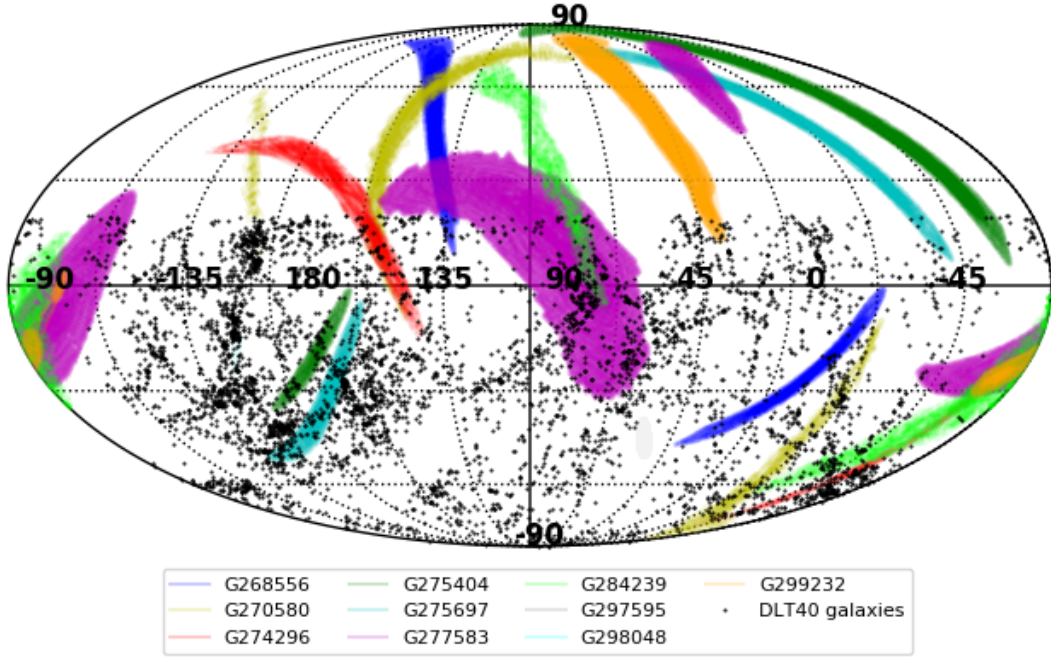


Table 1 (*continued*)

GW/GRB trigger	Source type	LVC GW estimations			D_{lum} (Mpc)	ref ^c	N_{gal}	DLT40 EM observations		REF ^e
		FAR ^a (yr ⁻¹)	Localization ^b (deg ²)	Obs_window (JD)				Detection ^d or r_{lim}		
2457892										
GW170608 (G288732)	CBC	2.6	860	320 ± 100	1
GW170809 (G296853)	CBC	0.25	1155	1000	m
GW170814 (G297595)	CBC	1/82800	97	550 ± 130	n	24	2457980-	19.0	G	
							2457982			
GW170817 (G298048)	CBC	1/9100	33.6	40 ± 8	o p	20	2457983-	DLT17ck	H I J	
GRB170817a					q	31	2457985	AT2017fgo (KN)		
G298389	Burst	6	799	...	r
GW170823 (G298936)	CBC	1/1800	2145	1387 ± 414	s
G299232	CBC	5.3	2040	339 ± 110	t	20	2457991-	19		
							2458005			

^aThe “FAR” column is the estimated false alarm rate per year, while the LVC threshold is one per month or 12 per year. If the FAR is less than 12, an alert would be issued.

^bThe “localization” column is the uncertainty area of GW triggers in 90% confidence level.

^ca.LIGO Scientific Collaboration & Virgo Collaboration (2017c); b.LIGO Scientific Collaboration & Virgo Collaboration (2017e); c.LIGO Scientific Collaboration & Virgo Collaboration (2017d); d.LIGO Scientific Collaboration & Virgo Collaboration (2017f); e.LIGO Scientific Collaboration & Virgo Collaboration (2017g); f.LIGO Scientific Collaboration & Virgo Collaboration (2017h); g.LIGO Scientific Collaboration & Virgo Collaboration (2017i); h.LIGO Scientific Collaboration & Virgo Collaboration (2017j); i.LIGO Scientific Collaboration & Virgo Collaboration (2017k); j.LIGO Scientific Collaboration & Virgo Collaboration (2017l); k.LIGO Scientific Collaboration & Virgo Collaboration (2017m); l.LIGO Scientific Collaboration & Virgo Collaboration (2017n); m.LIGO Scientific Collaboration & Virgo Collaboration (2017o); n.LIGO Scientific Collaboration & Virgo Collaboration (2017p); o.LIGO Scientific Collaboration & Virgo Collaboration (2017b); p.LIGO Scientific Collaboration & Virgo Collaboration (2017q); q.LIGO Scientific Collaboration & Virgo Collaboration (2017a); r.LIGO Scientific Collaboration & Virgo Collaboration (2017r); s.LIGO Scientific Collaboration & Virgo Collaboration (2017s); t.LIGO Scientific Collaboration & Virgo Collaboration (2017t).

^dWe report the typical DLT40 limiting magnitude (r band) for the observation set in the “Detection” column.

^eA.Yang et al. (2017a); B.Yang et al. (2017b); C.Yang et al. (2017c); D.Yang et al. (2017d); E.Yang et al. (2017e); F.Yang et al. (2017f); G.Yang et al. (2017g); H.Yang et al. (2017j); I.Yang et al. (2017i); J.Yang et al. (2017h).

^fFor GW170104 (G268556) and G270580 we only observed DLT40 galaxies out to 20 Mpc within the LVC localization as a test run.

4.1. G275404

G275404 was identified as a marginal GW candidate by the two LIGO interferometers, Hanford (H1) and Livingston (L1) using the pyCBC analysis (Usman et al. 2016) on 2017-02-25, 18:20:21.374 UTC (GPS time: 1172082639.374). The false-alarm rate of $1.89 \times 10^{-7} Hz$ corresponds to ~ 1 in 0.17 years. Following the initially-released bayestar localization map (Singer et al. 2016),

the 50% (90%) credible region spanned about 460 (2100) deg². DLT40 responded rapidly (within an hour) to select 50 galaxies within the LVC error region, which were observed from 2017-02-26 to 2017-03-09. At 2017-03-08 22:30:50 UTC (11 days after the initial trigger), the LALInference localization map (Veitch et al. 2015) was issued by the LVC with a 50% (90%) credible region which increased to about 2000 (17000) deg². Meanwhile, the LVC announced that the binary component

masses were estimated to be consistent with a binary neutron star (BNS) or NS-BH binary (LIGO Scientific Collaboration & Virgo Collaboration 2017i). Starting on 2017-03-09 (until 2017-03-12) we re-prioritized our targeted galaxy list, and observed 84 galaxies using the updated GW localization map. The first 50 galaxies represent 3.9% of all galaxies in the Glade catalogue within 40 Mpc and contain 12.7% of all B band luminosity of those galaxies; the latter 84 galaxies represent 1.5% of all galaxies and contains 9.7% of all B band luminosity. The typical DLT40 limiting magnitude for these observations was 19.2 mag (open filter scaled to r band).

We found one SN Ia, SN2017cbv/DLT17u, in NGC5643 (at a distance of $D \approx 12.3$ Mpc Sand et al. (2018) in the GW follow-up observations taken on 2017-03-08. Our follow-up observations of SN2017cbv/DLT17u with Las Cumbres Observatory telescopes show that SN2017cbv/DLT17u reached its maximum brightness ($B=11.79$ mag) 17.7 days after discovery (Hosseinzadeh et al. 2017). Given the typical rise time of SNe Ia (18.98 ± 0.54 days; Firth et al. 2015), we deduced that SN2017cbv was discovered very close to the explosion epoch and we can thus exclude SN2017cbv from being related to the GW event, which occurred ~ 2 weeks prior. Ultimately, further LVC analysis indicated that G275404 was not a trigger of interest (The LIGO Scientific Collaboration & the Virgo Collaboration 2019), confirming that SN 2017cbv was an unrelated transient.

4.2. GW170817/G298048

GW170817 (Abbott et al. 2017c,d) was identified by the LIGO H1 detector at August 17, 2017 12:41:04 UTC (GPS time: 1187008882.4457), as a likely BNS merger event. The false alarm rate was 3.478×10^{-12} Hz, equivalent to ~ 1 false alarm in 9100 years. In addition, the GW candidate was found in coincidence with the *Fermi*/GBM trigger 524666471/170817529 (GRB170817a; Goldstein et al. 2017), registered about 2 seconds later on Aug 17, 2017 12:41:06 UTC (GPS time: 1187008884.47). With further constraints from Virgo, the LVC joint sky area was reduced to 8.6 (33.6) deg 2 for the 50% (90%) credible regions, making it the best constrained event of the full O2 run. As shown in Figure 5, inside the 90% confidence region of GW170817 (33.6 deg 2), there were only 23 galaxies based on our DLT40 galaxy selection, and we decided to observe 20 of them (with 99% galaxy prioritization cut), together with the 31 most luminous galaxies in the GRB error-box region (*Fermi* GBM trigger). About ~ 11 hours after the announcement of the GW trigger, at the beginning of the Chilean night, DLT40 reported the detection of DLT17ck at RA=13:09:48.09 and DEC=

23:22:53.4.6, 5.37W, 8.60S arcsec from the center of NGC 4993 (Valenti et al. 2017; Yang et al. 2017j,i,h). Within one hour, we were one of the six optical groups which independently detected this optical transient, also named AT 2017 gfo and SSS17a (Abbott et al. 2017d; Coulter et al. 2017; Valenti et al. 2017; Tanvir et al. 2017; Lipunov et al. 2017; Soares-Santos et al. 2017a; Arcavi et al. 2017a). It was soon established that DLT17ck was a GW-associated kilonova (Li & Paczyński 1998; Pian et al. 2017; Villar et al. 2017; Evans et al. 2017; Metzger 2017; Kasen et al. 2017). No other transients were found in the other surveyed galaxies that DLT40 followed in the GW170817 localization region. The DLT40 follow-up data obtained for DLT17ck are described in Valenti et al. (2017). Yang et al. (2017) further used the observed light curve of DLT17ck to constrain the rate of BNS mergers to be less than 0.50 SNuB⁷ and we concluded that DLT40 would need to operate for ~ 18.4 years in order to discover a kilonova without a GW trigger.

4.3. Other GW triggers

GW170104/G268556 (Abbott et al. 2017a; LIGO Scientific Collaboration & Virgo Collaboration 2017c) was identified by L1 and H1 at 2017-01-04 10:11:58.599 UTC (GPS time: 1167559936.599). GW170104 was a BBH event with a low false-alarm rate, 6.1×10^{-8} Hz (about one in 6 months). This GW event was the first identified LVC trigger in the O2 run, and the first GW event followed by DLT40. The initial announcement of GW170104/G268556 did not include a distance estimate. For this first event, we decided to test our galaxy ranking algorithm and other infrastructure as a dry run, and not report our findings via a GCN. We monitored 18 galaxies within 20 Mpc for ~ 1 week within the 90% GW localization region, and no optical counterpart candidates were found.

G270580 (LIGO Scientific Collaboration & Virgo Collaboration 2017e,d) was identified by L1 and H1 at 2017-01-20 12:30:59.350 UTC (GPS time: 1168950677.350). The false alarm rate was 1.6×10^{-7} Hz (about one in 2.4 months). The 50% credible region spanned about 600 deg 2 and the 90% region about 3100 deg 2 . We observed 25 galaxies from the DLT40 catalogue within the 99% credible region, again within a distance of 20 Mpc, from 2017-01-23 onwards, for three weeks. No interesting transients were identified down to a typical limiting magnitude of 19.2 mag in r band (Yang et al. 2017a). This GW event was ultimately retracted by the LVC.

⁷ SNuB = 1 SN per 100 yr per $10^{10} L_{B,\odot}$

G274296 (LIGO Scientific Collaboration & Virgo Collaboration 2017f,g) was identified as a burst candidate by H1 and L1 at 2017-02-17 06:05:55.050 UTC (GPS time: 1171346771.050), with false alarm rate 1.7×10^{-7} Hz, or about one in 2 months. We observed 25 galaxies from our DLT40 galaxy catalogue (out to the full DLT40 $D=40$ Mpc search volume) within the 80.0% credible region of the trigger localization region. We began observing these galaxies on 2017-02-17 and monitored them for 3 weeks after the GW trigger. No interesting transients were identified down to an average limiting magnitude of 18.5 (Yang et al. 2017b). The LVC ultimately classified this GW trigger as of no further interest.

G275697 (LIGO Scientific Collaboration & Virgo Collaboration 2017j,k) was identified as a marginal candidate by L1 and H1 at 2017-02-27 18:57:31.375 UTC (GPS time: 1172257069.375), with a false alarm rate of 1.43×10^{-7} Hz or about one in 2 months. Based on a preliminary analysis, the LVC reported that the less massive component in the binary had a mass $< 3 M_{\odot}$ and that there was a 100% chance that the system ejected enough neutron-rich material to power an electromagnetic transient. The 50% credible region spanned about 480 deg 2 and the 90% region about 1800 deg 2 . The luminosity distance was estimated to be 181 ± 55 Mpc. We observed 59 galaxies from 2017-02-27 to 2017-03-07. After an update of the LVC localization map, we updated the galaxy sample and observed 114 galaxies from 2017-03-07 to 2017-03-12. No interesting transients were identified down to a limiting magnitude of ≈ 19.0 (Yang et al. 2017d). The final analysis of the LVC indicated that G275697 was not a trigger of interest.

G277583 (LIGO Scientific Collaboration & Virgo Collaboration 2017l) was identified as a burst candidate by L1 and H1 at 2017-03-13 22:40:09.593 UTC (GPS time: 1173480027.593). Its false alarm rate was 8.4×10^{-8} Hz (one in 4 months). We observed 55 galaxies within the 80.0% credible region, beginning on 2017-03-13 and continuing for 2 weeks after the GW trigger. No interesting transients were identified down to a limiting magnitude of 19.5 mag (Yang et al. 2017e). The final analysis of the LVC indicated that G277583 was not a trigger of interest.

G284239 (LIGO Scientific Collaboration & Virgo Collaboration 2017m) was identified by L1 and H1 at 2017-05-02 22:26:07.910 UTC (GPS time: 1177799185.910). G284239 was a low-significance short-duration burst candidate, whose false alarm rate was 1.26×10^{-7} Hz (4 per year). The 50% confidence region covered 1029 deg 2 and the 90% confidence region covered 3593 deg 2 . We observed 58 galaxies within the 95% credible region of the localization for a duration of two weeks starting on

2017-05-02 (Yang et al. 2017f). No interesting transients were identified down to a limiting magnitude of $r \sim 19$ mag. The LVC determined that this event was of no further interest.

G297595/GW170814 (LIGO Scientific Collaboration & Virgo Collaboration 2017p) was the first GW event detected by both the two LIGO detectors (H1, L1) and the Virgo (V1) detector (Abbott et al. 2017b) at 2017-08-14 10:30:43 UTC (GPS time: 1186741861.5268). The Virgo detection helped to decrease the 50% (90%) localization region from 333 (1158) deg 2 to 22 (97) deg 2 . GW170814 had a very low false alarm rate of 3.83×10^{-13} Hz, equivalent to ~ 1 per 82800 years. The LVC reported that the event was a BBH merger at $\sim 550 \pm 130$ Mpc. Despite the lack of an expected optical counterpart and the large distance, we triggered follow up partly because of the small localization region. We monitored 24 galaxies within the LVC error region with an average limiting magnitude of 19.0 mag (Yang et al. 2017g). No obvious optical counterparts were detected. All selected galaxies from this trigger were reset to normal priority on 2017 August 17 in order to aggressively pursue the next trigger, GW170817.

G299232 (LIGO Scientific Collaboration & Virgo Collaboration 2017t) was identified by L1 and H1 at 2017-08-25 13:13:31 UTC (GPS time: 1187702035.9831). G299232 was a low-significance candidate with a false alarm rate of 1.68×10^{-7} Hz (about 5.3 per year). The 50% credible region spanned about 450 deg 2 and the 90% region about 2040 deg 2 . We selected and observed 41 galaxies within 95.0% of the trigger localization region from 2017-08-25 to 2017-09-08. No obvious transient was found, and the LVC concluded that this event was of no further interest.

5. FUTURE PROSPECTS

In this section, we describe the DLT40 project's follow-up plans for the upcoming LVC O3 run based on some simple simulations of GW events, and the performance of DLT40.

5.1. DLT40 EM Counterpart Potential

To evaluate DLT40's potential impact for O3, we made use of the artificial star tests described in Yang et al. (2017), which provide point source detection efficiencies as a function of image zeropoint and seeing. Using these artificial star tests in conjunction with the real light curve of AT2017gfo/DLT17ck and the EM counterpart models shown in Figure 6, we calculate the limiting distance out to which the DLT40 program can detect each of these transients, as shown in Figure 8. Kilonovae with light curves similar to AT2017gfo/DLT17ck

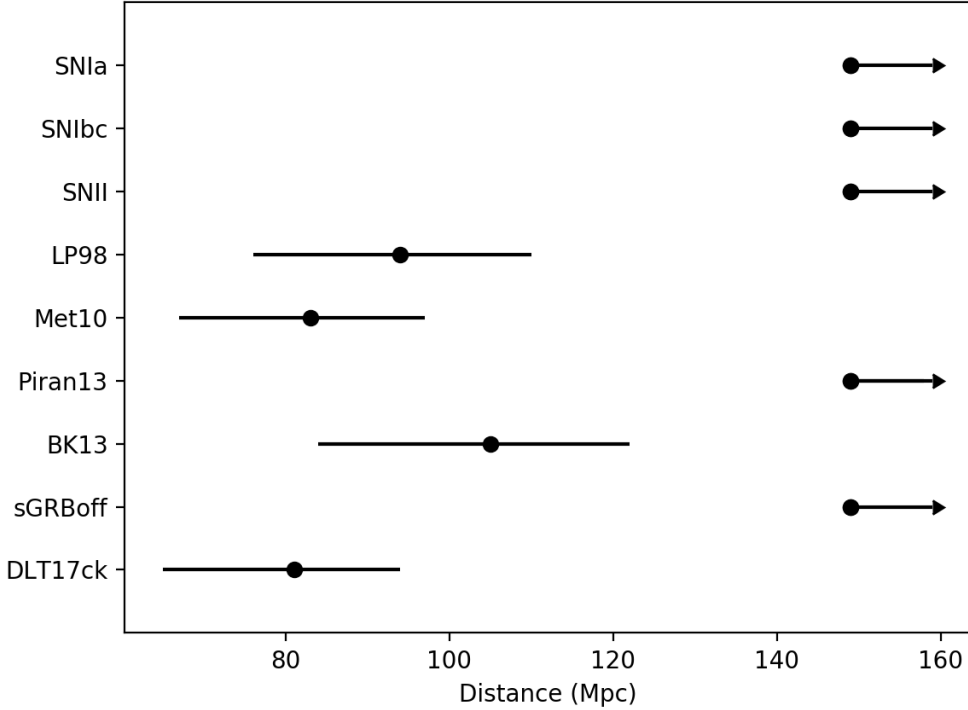


Figure 8. The DLT40 limiting distance for different BNS EM emission models (details described in Figure 6), and the observational data of DLT17ck, are estimated. The computational recipe is described as followed: 1. detection efficiency (DE) for single epoch/point: by setting up a series of artificial star experiments, we obtain the DE plots, which show the relations between the DLT40 detection efficiency, DE , with magnitude, for a specific field (Yang et al. 2017); 2. DE for epochs/sampling light curve: for a specific light curve (EM models or observations in absolute magnitudes), by executing step 1 for a sample of epochs ^a, we obtain DE_j for each epochs, while the overall DE is derived as $DE = 1 - \sum_j(1 - DE_j)$; 3. limiting distance estimation: we scaled each light curve to a distance of D_i , and obtain $DE_{D=D_i}$ at different distances. The limiting distance is then defined as the distance where $DE_{D=D_i}$ is 50%.

^a We decide the sample points by comparing the burst time of GW170817, with our DLT40 observing epochs towards NGC4993.

can be detected out to $D \approx 80$ Mpc, while other kilonova light curve models have similar limiting distances. For O3, the expected distance sensitivity of advanced LIGO to binary neutron star mergers will be $D \approx 120$ –170 Mpc, while for Virgo it will be $D \approx 65$ –85 Mpc (Abbott et al. 2016, 2018)⁸. If we assume that all kilonovae are as bright as AT2018gfo/DLT17ck and neglect that any potential galaxy catalog is incomplete, the current DLT40 observing strategy could detect all kilonovae in the Virgo volume during the O3 run. In the end, rather than going out to the full ≈ 80 Mpc distance horizon of Virgo for O3, we chose a distance at the lower end of their expected sensitivity ($D \approx 65$ Mpc), which was more

practical for the purposes of gathering template images of all the necessary galaxy fields.

5.2. DLT40 plans for O3

The DLT40 survey is continually upgrading its hardware and software, and we have been making special plans for the LVC O3 run – we summarize these improvements here.

- As shown in Section 5.1, the depth and cadence of DLT40 is suitable for finding typical kilonovae out to the horizon of the Virgo detector during O3. We are thus gathering template images of galaxies out to $D \approx 65$ Mpc (drawn from the GWGC, with $\text{Dec} < +20$ deg, $M_B < -18$ mag and $A_V < 0.5$ mag, as with the rest of the standard DLT40 search) in preparation for following up merger events with a neutron star in O3.

⁸ These distance ranges are the volume- and orientation-averaged distance at which a CBC of a given mass yields a matched filter signal-to-noise ratio (SNR) of 8 in a single detector.

2. The DLT40 team has recently added a second identical telescope to its SN search, located at Meckering Observatory in western Australia. This telescope will be utilized on an equal footing to the original DLT40 telescope at CTIO, and makes our GW counterpart search more robust to weather and instrument problems. It also decreases our response time to any given event, given our distributed longitudinal coverage. DLT40 is also in the process of incorporating a third telescope in Alberta, Canada, which will likely be operational near the currently planned start of O3 (April 2019). This telescope will provide northern hemisphere coverage for the DLT40 EM counterpart search.

3. Several recent improvements have been made to the overall DLT40 pipeline. Chief among them has been the adoption of a pixel-based, random forest machine learning algorithm used for scoring incoming SN candidates in real time (based on the algorithm used by the Pan-STARRS1 survey; Wright et al. 2015). This algorithm has drastically shrunk the number of transient candidates that must be inspected in a given night’s worth of data (~ 10 s instead of ~ 1000 s). In addition, very strong transient candidates with high machine learning scores trigger automated email alerts to the DLT40 team, which can respond with follow-up imaging on either DLT40 telescope within minutes.

4. The DLT40 GW follow-up code will respond autonomously to incoming LVC alerts, inserting the appropriate galaxy targets into the DLT40 scheduler at high priority in real time. It will also alert the team if a counterpart candidate appears in a selected field (see point (iii) above). DLT40 will respond to all burst alerts in O3 (which will not have distance information) as well as all CBC alerts which have a cumulative probability of $>10\%$ of being within $D < 65$ Mpc (we intend to follow all nearby CBC alerts. In case the trigger rate is relatively high in O3, e.g. several sources within one week, we would manually evaluate them with the false alarm rate and the probability of which contains a neutron star).

6. SUMMARY

We have presented the GW follow-up strategy and results for the DLT40 survey during the O2 observing run of Advanced LIGO and Virgo. DLT40 employed a galaxy-targeted search which combined the GW localization region and the galaxy catalog employed by the DLT40 SN search to prioritize targets for follow-up. This strategy bore fruit for GW170817, the first detected binary neutron star merger, as DLT40 co-discovered the associated kilonova AT2017gfo/SSS17a/DLT17ck (Valenti et al. 2017). In all, we present follow-up observations of ten out of the sixteen O2 GW triggers. Of these ten, three events were ultimately verified as *bona fide* GW events.

Finally, in Section 5 we discussed the DLT40 team’s follow-up plans for the upcoming O3 detector run. Two additional, identical telescopes will be added in Australia and Canada, providing longitudinal and northern hemisphere coverage. Automated response to new GW events will allow for immediate scheduling of high-priority galaxy fields on one of DLT40’s search telescopes, and a new machine learning algorithm will cleanly identify new transient events and notify the team within minutes if a strong optical counterpart candidate is found. Further, artificial star experiments indicate that DLT40 will be sensitive to kilonovae out to the neutron star merger horizon of Virgo during O3, and we will respond to any appropriate event out to $D \approx 65$ Mpc. Small robotic telescope systems, coupled with smart software, will continue to have an out-sized impact on multi-messenger astrophysics in the years ahead.

ACKNOWLEDGEMENTS

SY would like to thank Marica Branchesi and He Gao for helpful discussions and comments. SY acknowledges from the China Scholarship Council #201506040044, and the supported by the PRIN-INAF 2016 with the project ”Towards the SKA and CTA era: discovery, localization, and physics of transient source”. Research by DJS is supported by NSF grants AST-1821967, 1821987, 1813708 and 1813466. Research by SV is supported by NSF grant AST-1813176. The DLT40 web-pages structure were developed at the Aspen Center for Physics, which is supported by National Science Foundation grant PHY-1066293. AC acknowledges support from the NSF award #1455090 ”CAREER: Radio and gravitational-wave emission from the largest explosions since the Big Bang”.

REFERENCES

Aasi, J., Abadie, J., Abbott, B. P., et al. 2015, Classical and Quantum Gravity, 32, 115012

Abbott, B. P., Abbott, R., Abbott, T. D., et al. 2016a, Physical Review X, 6, 041015

- . 2016b, Physical Review Letters, 116, 241103
- . 2016c, ApJL, 826, L13
- . 2016d, ApJL, 826, L13
- . 2016e, Phys. Rev. Lett., 116, 061102
- Abbott, B. P., The LIGO Scientific Collaboration, Virgo Collaboration, et al. 2016, Living Reviews in Relativity, 19, 1
- Abbott, B. P., Abbott, R., Abbott, T. D., et al. 2017a, Phys. Rev. Lett., 118, 221101
- . 2017b, Physical Review Letters, 119, 141101
- . 2017c, Phys. Rev. Lett., 119, 161101
- . 2017d, ApJL, 848, L12
- Abbott, B. P., Abbott, R., Abbott, T. D., et al. 2018, Living Reviews in Relativity, 21, 3
- Acernese, F., Agathos, M., Agatsuma, K., et al. 2015, Classical and Quantum Gravity, 32, 024001
- Arcavi, I., Hosseinzadeh, G., Howell, D. A., et al. 2017a, Nature, 551, 64
- Arcavi, I., McCully, C., Hosseinzadeh, G., et al. 2017b, ApJL, 848, L33
- Barnes, J., & Kasen, D. 2013, ApJ, 775, 18
- Bartos, I., Kocsis, B., Haiman, Z., & Márka, S. 2017, ApJ, 835, 165
- Becker, A. 2015, HOTPANTS: High Order Transform of PSF ANd Template Subtraction, Astrophysics Source Code Library, , , ascl:1504.004
- Bertin, E., & Arnouts, S. 1996, A&AS, 117, 393
- Brown, T. M., Baliber, N., Bianco, F. B., et al. 2013, PASP, 125, 1031
- Connaughton, V., Burns, E., Goldstein, A., et al. 2016, ApJ, 826, L6
- Coulter, D. A., Foley, R. J., Kilpatrick, C. D., et al. 2017, Science, 358, 1556
- Dálya, G., Galgócz, G., Dobos, L., et al. 2018, MNRAS, 479, 2374
- de Mink, S. E., & King, A. 2017, ApJL, 839, L7
- Doctor, Z., Kessler, R., Herner, K., et al. 2018, ArXiv e-prints, arXiv:1812.01579
- Evans, P. A., Cenko, S. B., Kennea, J. A., et al. 2017, Science, 358, 1565
- Firth, R. E., Sullivan, M., Gal-Yam, A., et al. 2015, Monthly Notices of the Royal Astronomical Society, 446, 3895
- Fong, W., & Berger, E. 2013, ApJ, 776, 18
- Gehrels, N., Cannizzo, J. K., Kanner, J., et al. 2016, ApJ, 820, 136
- Goldstein, A., Veres, P., Burns, E., et al. 2017, ApJL, 848, L14
- Goldstein, A., Veres, P., Burns, E., et al. 2017, The Astrophysical Journal Letters, 848, L14
- Haggard, D., Nynka, M., Ruan, J. J., et al. 2017, ApJL, 848, L25
- Hallinan, G., Corsi, A., Mooley, K. P., et al. 2017, Science, 358, 1579
- Hosseinzadeh, G., Sand, D. J., Valenti, S., et al. 2017, ApJL, 845, L11
- Kasen, D., Badnell, N. R., & Barnes, J. 2013, ApJ, 774, 25
- Kasen, D., Metzger, B., Barnes, J., Quataert, E., & Ramirez-Ruiz, E. 2017, Nature, 551, 80
- Kasliwal, M. M., Cenko, S. B., Singer, L. P., et al. 2016, ApJL, 824, L24
- Li, L.-X., & Paczyński, B. 1998, ApJL, 507, L59
- LIGO Scientific Collaboration, & Virgo Collaboration. 2017a, GRB Coordinates Network, 21505
- . 2017b, GRB Coordinates Network, 21510
- . 2017c, GRB Coordinates Network, 20364
- . 2017d, GRB Coordinates Network, 21281
- . 2017e, GRB Coordinates Network, 20486
- . 2017f, GRB Coordinates Network, 20689
- . 2017g, GRB Coordinates Network, 21284
- . 2017h, GRB Coordinates Network, 20738
- . 2017i, GRB Coordinates Network, 20840
- . 2017j, GRB Coordinates Network, 20763
- . 2017k, GRB Coordinates Network, 20833
- . 2017l, GRB Coordinates Network, 20860
- . 2017m, GRB Coordinates Network, 21060
- . 2017n, GRB Coordinates Network, 21221
- . 2017o, GRB Coordinates Network, 21431
- . 2017p, GRB Coordinates Network, 21474
- . 2017q, GRB Coordinates Network, 21513
- . 2017r, GRB Coordinates Network, 21656
- . 2017s, GRB Coordinates Network, 21600
- . 2017t, GRB Coordinates Network, 21693
- Lipunov, V. M., Gorbovskoy, E., Kornilov, V. G., et al. 2017, The Astrophysical Journal Letters, 850, L1
- Loeb, A. 2016, ApJ, 819, L21
- Margutti, R., Berger, E., Fong, W., et al. 2017, ApJL, 848, L20
- Marion, G. H., Brown, P. J., Vinkó, J., et al. 2016, ApJ, 820, 92
- Metzger, B. D. 2017, Living Reviews in Relativity, 20, 3
- Metzger, B. D., Martínez-Pinedo, G., Darbha, S., et al. 2010, MNRAS, 406, 2650
- Perna, R., Chruslinska, M., Corsi, A., & Belczynski, K. 2018, MNRAS, 477, 4228
- Perna, R., Lazzati, D., & Giacomazzo, B. 2016, ApJ, 821, L18
- Pian, E., D'Avanzo, P., Benetti, S., et al. 2017, Nature, 551, 67

- Piran, T., Nakar, E., & Rosswog, S. 2013, MNRAS, 430, 2121
- Reichart, D., Nysewander, M., Moran, J., et al. 2005, Nuovo Cimento C Geophysics Space Physics C, 28, 767
- Sand, D. J., Graham, M. L., Botyánszki, J., et al. 2018, ApJ, 863, 24
- Savchenko, V., Ferrigno, C., Kuulkers, E., et al. 2017, ApJL, 848, L15
- Singer, L. P., & Price, L. R. 2016, PhRvD, 93, 024013
- Singer, L. P., Chen, H.-Y., Holz, D. E., et al. 2016, ApJL, 829, L15
- Smartt, S. J., Chambers, K. C., Smith, K. W., et al. 2016, MNRAS, 462, 4094
- Soares-Santos, M., Holz, D. E., Annis, J., et al. 2017a, ApJL, 848, L16
- . 2017b, ApJL, 848, L16
- Tanvir, N. R., Levan, A. J., González-Fernández, C., et al. 2017, ApJ, 848, L27
- Tartaglia, L., Sand, D. J., Valenti, S., et al. 2018, ApJ, 853, 62
- The LIGO Scientific Collaboration, & the Virgo Collaboration. 2019, arXiv e-prints, arXiv:1901.03310
- Troja, E., Piro, L., van Eerten, H., et al. 2017, Nature, 551, 71
- Usman, S. A., Nitz, A. H., Harry, I. W., et al. 2016, Classical and Quantum Gravity, 33, 215004
- Valenti, S., David, Sand, J., et al. 2017, ApJL, 848, L24
- van Eerten, H. J., & MacFadyen, A. I. 2011, ApJL, 733, L37
- Veitch, J., Raymond, V., Farr, B., et al. 2015, Phys. Rev. D, 91, 042003
- Villar, V. A., Guillochon, J., Berger, E., et al. 2017, ApJ, 851, L21
- White, D. J., Daw, E. J., & Dhillon, V. S. 2011, Classical and Quantum Gravity, 28, 085016
- Wright, D. E., Smartt, S. J., Smith, K. W., et al. 2015, MNRAS, 449, 451
- Yang, S., Valenti, S., Sand, D., & et al. 2017a, GRB Coordinates Network, 20669
- . 2017b, GRB Coordinates Network, 20875
- . 2017c, GRB Coordinates Network, 21010
- . 2017d, GRB Coordinates Network, 20876
- . 2017e, GRB Coordinates Network, 21009
- . 2017f, GRB Coordinates Network, 21116
- . 2017g, GRB Coordinates Network, 21878
- . 2017h, GRB Coordinates Network, 21579
- . 2017i, GRB Coordinates Network, 21539
- . 2017j, GRB Coordinates Network, 21531
- Yang, S., Valenti, S., Cappellaro, E., et al. 2017, ApJL, 851, L48
- Yuan, F., Jerkstrand, A., Valenti, S., et al. 2016, MNRAS, 461, 2003
- Zhang, S.-N., Liu, Y., Yi, S., Dai, Z., & Huang, C. 2016, ArXiv e-prints, arXiv:1604.02537

APPENDIX

A. DLT40 GW FOLLOW-UP OBSERVING LOGS FOR THE LVC O2 RUN

Table 2, 3, 4, 5, 6, 7, 8, 9, 10, 11, 12, 13, 14 present the DLT40 galaxies that were selected, activated and followed by us during the second observing run of the LVC. In each of the presented galaxy lists, we display target galaxy information (from the GWGC; White et al. 2011) including the galaxy name, equatorial coordinates, luminosity distance, and absolute magnitude in B and K band. We also include details of the observations, including the observing window, and the score estimated by our DLT40 galaxy prioritization algorithm. These information was also presented in the DLT40 team’s O2 GCNs.

Table 2. Galaxies observed after trigger GW170104/G268556. Table columns provide the galaxy name, coordinates, distance, B and K-band magnitude, observing window and the score from our ranking algorithm. The cumulative score is 0.357.

Name (1)	RA(J2000) (2)	DEC(J2000) (3)	Dist(Mpc) (4)	B(mag) (5)	K(mag) (6)	OBS_WINDOW(JD) (7)	SCORE (8)
NGC7507	348.03	-28.54	25.00	-20.77	-24.70	2457759.33-2457766.29	2.033×10^{-1}
NGC7755	356.97	-30.52	27.92	-20.63	-23.26	2457759.33-2457766.29	6.838×10^{-2}
NGC1291	49.33	-41.11	10.38	-20.66	-24.42	2457759.33-2457766.29	1.823×10^{-2}
NGC1448	56.13	-44.64	15.35	-20.30	-23.27	2457759.33-2457766.29	1.013×10^{-2}
NGC1365	53.40	-36.14	17.95	-21.39	-24.90	2457759.33-2457766.29	8.132×10^{-3}
NGC2263	99.62	-24.85	32.36	-20.75	-23.41	2457759.33-2457766.29	5.403×10^{-3}
NGC1411	54.69	-44.10	19.77	-19.78	-23.33	2457759.33-2457766.29	5.345×10^{-3}
ESO557-009	99.68	-20.29	32.08	-20.52	-21.91	2457759.33-2457766.29	4.550×10^{-3}
IC0438	88.25	-17.88	36.64	-20.33	-23.12	2457759.33-2457766.29	4.188×10^{-3}
NGC7713A	354.28	-37.71	36.67	-20.15	-22.27	2457759.33-2457766.29	3.945×10^{-3}
NGC2217	95.42	-27.23	20.80	-20.31	-24.50	2457759.33-2457766.29	3.910×10^{-3}
NGC2350	108.30	12.27	28.84	-20.00	-23.04	2457759.33-2457766.29	3.750×10^{-3}
NGC2089	86.96	-17.60	38.11	-20.33	-24.09	2457759.33-2457766.29	3.740×10^{-3}
IC2143	86.72	-18.73	38.02	-20.12	-23.20	2457759.33-2457766.29	3.546×10^{-3}
PGC018581	92.78	-15.49	24.21	-19.87	-21.74	2457759.33-2457766.29	2.972×10^{-3}
PGC085930	99.80	-1.51	36.83	-20.43	-23.90	2457759.33-2457766.29	2.850×10^{-3}
NGC7371	341.52	-11.00	29.92	-19.74	-23.14	2457759.33-2457766.29	2.437×10^{-3}
NGC2377	111.24	-9.66	29.92	-20.17	-23.37	2457759.33-2457766.29	2.330×10^{-3}

Table 3. Galaxies observed after trigger G270580. Table columns provide the galaxy name, coordinates, distance, B and K-band magnitude, observing window and the score from our ranking algorithm. The cumulative score is 0.106.

Name (1)	RA(J2000) (2)	DEC(J2000) (3)	Dist(Mpc) (4)	B(mag) (5)	K(mag) (6)	OBS_WINDOW(JD) (7)	SCORE (8)
NGC4419	186.74	15.05	13.49	-19.24	-22.91	2457991.48-2458005.21	2.703×10^{-2}
NGC4216	183.98	13.15	14.13	-20.58	-24.23	2457991.48-2458005.21	1.633×10^{-2}
IC5201	335.24	-46.03	9.20	-18.78	-19.65	2457991.48-2458005.21	9.84×10^{-3}
NGC4571	189.23	14.22	14.93	-19.12	-22.35	2457991.48-2458005.21	9.603×10^{-3}
NGC4498	187.91	16.85	14.06	-18.54	-21.08	2457991.48-2458005.21	9.24×10^{-3}
NGC4192	183.45	14.90	13.61	-20.62	-23.78	2457991.48-2458005.21	5.19×10^{-3}
NGC4178	183.19	10.87	14.00	-19.37	-21.16	2457991.48-2458005.21	5.118×10^{-3}
NGC1546	63.65	-56.06	13.87	-18.21	-22.66	2457991.48-2458005.21	4.41×10^{-3}
NGC0253	11.89	-25.29	3.94	-20.06	-24.21	2457991.48-2458005.21	3.267×10^{-3}
NGC1559	64.40	-62.78	12.59	-19.85	-22.48	2457991.48-2458005.21	2.509×10^{-3}
NGC1566	65.00	-54.94	6.55	-18.89	-22.20	2457991.48-2458005.21	1.830×10^{-3}
NGC2640	129.35	-55.12	12.71	-20.17	-23.81	2457991.48-2458005.21	1.770×10^{-3}
NGC1947	81.70	-63.76	13.87	-19.01	-23.21	2457991.48-2458005.21	1.323×10^{-3}
NGC4123	182.05	2.88	14.86	-19.09	-22.07	2457991.48-2458005.21	1.072×10^{-3}
NGC1617	67.92	-54.60	13.87	-19.79	-23.63	2457991.48-2458005.21	1.017×10^{-3}
NGC1602	66.98	-55.06	13.69	-18.48	-18.66	2457991.48-2458005.21	9.102×10^{-4}
IC2056	64.10	-60.21	15.00	-18.48	-21.73	2457991.48-2458005.21	8.838×10^{-4}
NGC1796	75.68	-61.14	15.00	-18.28	-21.18	2457991.48-2458005.21	7.911×10^{-4}
NGC7090	324.12	-54.56	6.28	-18.56	-20.83	2457991.48-2458005.21	6.363×10^{-4}
ESO097-013	213.29	-65.34	4.21	-19.03	-23.14	2457991.48-2458005.21	6.333×10^{-4}
NGC1249	47.51	-53.34	14.19	-19.16	-21.41	2457991.48-2458005.21	5.976×10^{-4}
NGC3521	166.45	-0.04	11.22	-20.85	-24.47	2457991.48-2458005.21	5.433×10^{-4}
ESO494-026	121.55	-27.53	14.15	-19.86	-22.88	2457991.48-2458005.21	2.601×10^{-4}
IC1954	52.88	-51.90	13.68	-18.98	-21.93	2457991.48-2458005.21	2.021×10^{-4}
NGC1313	49.56	-66.50	4.07	-18.79	-20.48	2457991.48-2458005.21	1.706×10^{-4}
ESO054-021	57.46	-71.63	13.87	-18.85	-20.36	2457991.48-2458005.21	1.467×10^{-4}
NGC7814	0.81	16.15	13.18	-19.68	-23.52	2457991.48-2458005.21	1.438×10^{-4}
NGC2784	138.08	-24.17	9.82	-19.42	-23.64	2457991.48-2458005.21	9.909×10^{-5}
NGC2835	139.47	-22.35	8.05	-19.03	-21.61	2457991.48-2458005.21	8.748×10^{-5}
NGC0014	2.19	15.82	13.87	-18.61	-20.29	2457991.48-2458005.21	6.519×10^{-5}
NGC0428	18.23	0.98	14.79	-19.12	-21.46	2457991.48-2458005.21	5.913×10^{-5}
NGC2283	101.47	-18.21	9.86	-18.17	-19.85	2457991.48-2458005.21	3.786×10^{-5}
PGC018855	95.23	-8.50	11.22	-18.39	-21.94	2457991.48-2458005.21	3.753×10^{-5}

Table 4. Galaxies observed after trigger G274296. Table columns provide the galaxy name, coordinates, distance, B and K-band magnitude, observing window and the score from our ranking algorithm. The cumulative score is 0.704.

Name (1)	RA(J2000) (2)	DEC(J2000) (3)	Dist(Mpc) (4)	B(mag) (5)	K(mag) (6)	OBS_WINDOW(JD) (7)	SCORE (8)
IC4837A	288.82	-54.13	33.42	-21.15	-24.47	2457802.38-2457825.37	4.803×10^{-2}
IC4837	288.81	-54.67	33.42	-20.72	-20.38	2457802.38-2457825.37	3.770×10^{-2}
IC4839	288.89	-54.63	35.11	-20.02	-23.48	2457802.38-2457825.37	3.770×10^{-2}
NGC3041	148.28	16.68	23.77	-19.86	-23.14	2457802.38-2457825.37	3.738×10^{-2}
NGC6788	291.71	-54.95	34.56	-21.09	-24.17	2457802.38-2457825.37	3.607×10^{-2}
NGC2698	133.90	-3.18	24.94	-18.89	-23.14	2457802.38-2457825.37	3.437×10^{-2}
NGC2708	134.03	-3.36	26.55	-19.15	-23.24	2457802.38-2457825.37	3.437×10^{-2}
NGC2697	133.75	-2.99	24.17	-18.59	-22.02	2457802.38-2457825.37	3.041×10^{-2}
NGC2695	133.61	-3.07	32.36	-19.76	-23.70	2457802.38-2457825.37	3.041×10^{-2}
NGC2706	134.05	-2.56	21.88	-18.48	-22.18	2457802.38-2457825.37	2.778×10^{-2}
NGC2775	137.58	7.04	17.30	-20.17	-24.15	2457802.38-2457825.37	2.725×10^{-2}
NGC2919	143.70	10.28	34.67	-19.54	-22.65	2457802.38-2457825.37	2.151×10^{-2}
NGC2722	134.69	-3.71	38.02	-19.68	-22.49	2457802.38-2457825.37	2.111×10^{-2}
IC0540	142.54	7.90	28.64	-18.75	-21.77	2457802.38-2457825.37	2.010×10^{-2}
NGC2690	133.16	-2.60	21.04	-18.61	-21.97	2457802.38-2457825.37	1.944×10^{-2}
NGC2906	143.03	8.44	29.92	-19.28	-23.27	2457802.38-2457825.37	1.905×10^{-2}
NGC2894	142.38	7.72	30.49	-19.75	-23.31	2457802.38-2457825.37	1.814×10^{-2}
NGC6810	295.89	-58.66	23.12	-20.42	-24.14	2457802.38-2457825.37	1.742×10^{-2}
NGC3226	155.86	19.90	23.55	-19.59	-23.29	2457802.38-2457825.37	1.741×10^{-2}
UGC05467	152.05	18.71	39.71	-18.96	-22.15	2457802.38-2457825.37	1.220×10^{-2}
IC4821	287.38	-55.02	25.00	-18.98	-21.61	2457802.38-2457825.37	1.144×10^{-2}
IC2367	126.04	-18.78	29.18	-20.71	-23.89	2457802.38-2457825.37	1.141×10^{-2}
IC4797	284.12	-54.31	28.05	-20.23	-24.17	2457802.38-2457825.37	1.103×10^{-2}
PGC024778	132.25	-7.83	38.02	-19.75	-22.33	2457802.38-2457825.37	9.475×10^{-3}
NGC6920	310.99	-80.00	32.99	-20.52	-24.22	2457802.38-2457825.37	9.363×10^{-3}
UGC05403	150.65	19.18	33.42	-18.48	-22.28	2457802.38-2457825.37	9.153×10^{-3}
ESO231-017	286.19	-47.85	35.14	-19.62	-23.20	2457802.38-2457825.37	8.543×10^{-3}
NGC6844	300.71	-65.23	36.98	-19.60	-23.47	2457802.38-2457825.37	7.537×10^{-3}
IC4889	296.31	-54.34	29.24	-20.33	-24.22	2457802.38-2457825.37	7.368×10^{-3}
PGC023658	126.49	-11.78	38.93	-19.84	-21.71	2457802.38-2457825.37	7.059×10^{-3}
NGC3020	147.53	12.81	21.88	-19.20	-21.02	2457802.38-2457825.37	6.063×10^{-3}
NGC3024	147.61	12.77	25.35	-18.92	-20.84	2457802.38-2457825.37	6.063×10^{-3}
PGC023723	126.89	-12.76	34.61	-19.08	-21.69	2457802.38-2457825.37	5.956×10^{-3}
UGC04684	134.17	0.38	35.67	-18.54	-20.52	2457802.38-2457825.37	5.682×10^{-3}
IC4871	293.93	-57.52	22.59	-18.80	-20.88	2457802.38-2457825.37	5.112×10^{-3}
IC4901	298.60	-58.71	17.86	-19.61	-22.41	2457802.38-2457825.37	4.946×10^{-3}
IC4817	286.55	-56.16	33.42	-18.96	-21.27	2457802.38-2457825.37	4.438×10^{-3}
IC5071	315.33	-72.64	30.90	-19.65	-22.94	2457802.38-2457825.37	4.270×10^{-3}

Table 4 continued

Table 4 (*continued*)

Name (1)	RA(J2000) (2)	DEC(J2000) (3)	Dist(Mpc) (4)	B(mag) (5)	K(mag) (6)	OBS_WINDOW(JD) (7)	SCORE (8)
IC5026	312.12	-78.07	32.36	-19.16	-20.55	2457802.38-2457825.37	3.636×10^{-3}
NGC2612	128.46	-13.17	21.67	-18.59	-22.90	2457802.38-2457825.37	3.557×10^{-3}
IC4964	304.35	-73.89	39.26	-18.72	-21.34	2457802.38-2457825.37	2.934×10^{-3}
IC4885	295.97	-60.65	29.92	-18.39	-21.35	2457802.38-2457825.37	2.844×10^{-3}
UGC04845	138.11	9.96	30.18	-18.33	-20.68	2457802.38-2457825.37	2.502×10^{-3}
ESO027-003	328.43	-81.65	30.64	-18.88	-18.75	2457802.38-2457825.37	2.216×10^{-3}
ESO027-008	335.77	-80.00	21.88	-18.73	-22.39	2457802.38-2457825.37	2.100×10^{-3}
ESO027-001	328.11	-81.53	29.92	-20.10	-23.21	2457802.38-2457825.37	1.780×10^{-3}

Table 5. Galaxies observed after trigger G275404 (with the preliminary bayestar localization map). Table columns provide the galaxy name, coordinates, distance, B and K-band magnitude, observing window and the score from our ranking algorithm. The cumulative score is 0.621.

Name (1)	RA(J2000) (2)	DEC(J2000) (3)	Dist(Mpc) (4)	B(mag) (5)	K(mag) (6)	OBS_WINDOW(JD) (7)	SCORE (8)
NGC3923	177.76	-28.81	22.91	-20.97	-25.30	2457810.63-2457821.57	4.229×10^{-2}
NGC3904	177.30	-29.28	28.31	-20.53	-24.58	2457810.63-2457821.57	3.748×10^{-2}
ESO440-027	178.35	-28.55	18.53	-18.93	-21.74	2457810.63-2457821.57	3.080×10^{-2}
ESO440-011	177.19	-28.29	21.88	-19.21	-18.05	2457810.63-2457821.57	2.991×10^{-2}
IC3010	181.99	-30.34	25.87	-19.21	-22.86	2457810.63-2457821.57	2.848×10^{-2}
IC3005	181.81	-30.02	24.32	-19.01	-21.96	2457810.63-2457821.57	2.618×10^{-2}
NGC4105	181.67	-29.76	26.55	-20.32	-24.60	2457810.63-2457821.57	2.421×10^{-2}
ESO441-014	182.56	-30.08	24.67	-18.60	-19.56	2457810.63-2457821.57	2.245×10^{-2}
IC3253	185.94	-34.62	34.67	-21.00	-23.59	2457810.63-2457821.57	2.235×10^{-2}
IC2996	181.45	-29.97	21.88	-18.47	-20.65	2457810.63-2457821.57	2.205×10^{-2}
NGC3885	176.69	-27.92	21.88	-19.72	-23.33	2457810.63-2457821.57	2.126×10^{-2}
IC0764	182.56	-29.74	21.18	-20.13	-21.92	2457810.63-2457821.57	2.064×10^{-2}
ESO440-004	176.42	-28.37	22.93	-18.82	-18.47	2457810.63-2457821.57	1.781×10^{-2}
ESO441-017	182.78	-31.13	24.24	-19.97	-21.10	2457810.63-2457821.57	1.721×10^{-2}
IC3015	182.25	-31.52	24.21	-19.53	-23.11	2457810.63-2457821.57	1.707×10^{-2}
NGC4304	185.55	-33.48	34.67	-20.24	-23.65	2457810.63-2457821.57	1.664×10^{-2}
NGC3459	163.68	-17.04	31.61	-20.25	-22.44	2457810.63-2457821.57	1.566×10^{-2}
IC0760	181.47	-29.29	25.37	-19.23	-22.63	2457810.63-2457821.57	1.539×10^{-2}
PGC086291	283.00	11.88	38.02	-20.63	-24.07	2457810.63-2457821.57	1.298×10^{-2}
ESO440-049	181.39	-31.42	24.24	-18.99	-20.12	2457810.63-2457821.57	1.209×10^{-2}
ESO380-019	185.51	-35.79	38.02	-20.37	-24.24	2457810.63-2457821.57	1.140×10^{-2}
PGC033108	164.91	-15.53	35.63	-20.04	-21.28	2457810.63-2457821.57	1.082×10^{-2}

Table 5 continued

Table 5 (*continued*)

Name (1)	RA(J2000) (2)	DEC(J2000) (3)	Dist(Mpc) (4)	B(mag) (5)	K(mag) (6)	OBS_WINDOW(JD) (7)	SCORE (8)
NGC3321	159.71	-11.65	33.88	-19.85	-22.17	2457810.63-2457821.57	1.002×10^{-2}
NGC3936	178.09	-26.91	18.62	-19.55	-22.28	2457810.63-2457821.57	9.942×10^{-3}
ESO380-050	189.59	-35.62	38.02	-20.13	-20.51	2457810.63-2457821.57	8.576×10^{-3}
ESO504-028	178.73	-27.25	22.24	-18.89	-20.30	2457810.63-2457821.57	7.981×10^{-3}
NGC4947	196.33	-35.34	27.80	-20.32	-23.20	2457810.63-2457821.57	7.905×10^{-3}
PGC032091	161.30	-10.06	27.64	-18.64	-20.17	2457810.63-2457821.57	6.998×10^{-3}
ESO440-038	180.43	-31.70	26.65	-19.10	-22.02	2457810.63-2457821.57	6.523×10^{-3}
NGC3375	161.75	-9.94	28.87	-19.54	-22.53	2457810.63-2457821.57	5.771×10^{-3}
NGC3361	161.12	-11.21	24.21	-19.13	-21.86	2457810.63-2457821.57	5.756×10^{-3}
PGC031979	160.90	-9.86	24.21	-18.32	-19.86	2457810.63-2457821.57	5.567×10^{-3}
NGC3055	148.83	4.27	25.35	-19.54	-22.53	2457810.63-2457821.57	5.334×10^{-3}
UGC05347	149.32	4.53	29.92	-19.03	-20.24	2457810.63-2457821.57	5.171×10^{-3}
IC2627	167.47	-23.73	24.21	-19.62	-22.93	2457810.63-2457821.57	5.125×10^{-3}
ESO441-012	182.36	-32.52	24.21	-18.28	-21.73	2457810.63-2457821.57	4.921×10^{-3}
NGC5121	201.19	-37.68	20.80	-19.59	-23.13	2457810.63-2457821.57	4.883×10^{-3}
NGC3044	148.42	1.58	21.68	-19.85	-22.70	2457810.63-2457821.57	4.768×10^{-3}
NGC3617	169.46	-26.13	25.61	-18.91	-22.26	2457810.63-2457821.57	4.067×10^{-3}
IC0630	159.64	-7.17	25.85	-19.72	-23.41	2457810.63-2457821.57	3.970×10^{-3}
ESO381-029	194.12	-36.37	29.54	-19.39	-22.62	2457810.63-2457821.57	3.914×10^{-3}
ESO440-037	179.82	-28.90	22.99	-18.26	-20.92	2457810.63-2457821.57	3.717×10^{-3}
IC2995	181.45	-27.94	16.75	-19.42	-21.80	2457810.63-2457821.57	3.706×10^{-3}
NGC3673	171.30	-26.74	17.38	-19.20	-22.65	2457810.63-2457821.57	3.586×10^{-3}
ESO324-044	204.53	-39.84	34.51	-19.70	-21.85	2457810.63-2457821.57	3.514×10^{-3}
NGC3511	165.85	-23.09	12.25	-19.64	-22.37	2457810.63-2457821.57	3.494×10^{-3}
ESO324-023	201.87	-38.18	14.26	-18.21	-19.15	2457810.63-2457821.57	3.151×10^{-3}
UGC05376	150.11	3.37	29.92	-18.81	-22.60	2457810.63-2457821.57	2.772×10^{-3}
ESO569-014	162.85	-19.89	24.77	-19.33	-20.98	2457810.63-2457821.57	2.756×10^{-3}
ESO381-038	195.02	-34.43	28.37	-18.70	-20.39	2457810.63-2457821.57	2.425×10^{-3}

Table 6. Galaxies observed after trigger G275404 (with the updated LALInference localization map). Table columns provide the galaxy name, coordinates, distance, B and K-band magnitude, observing window and the score from our ranking algorithm. The cumulative score is 0.243.

Name (1)	RA(J2000) (2)	DEC(J2000) (3)	Dist(Mpc) (4)	B(mag) (5)	K(mag) (6)	OBS_WINDOW(JD) (7)	SCORE (8)
NGC3923	177.76	-28.81	22.91	-20.97	-25.30	2457821.57-2457825.39	1.209×10^{-2}
NGC3904	177.30	-29.28	28.31	-20.53	-24.58	2457821.57-2457825.39	1.112×10^{-2}

Table 6 continued

Table 6 (*continued*)

Name (1)	RA(J2000) (2)	DEC(J2000) (3)	Dist(Mpc) (4)	B(mag) (5)	K(mag) (6)	OBS_WINDOW(JD) (7)	SCORE (8)
ESO380-006	183.89	-35.63	38.93	-21.31	-24.79	2457821.57-2457825.39	8.775×10^{-3}
NGC4603	190.23	-40.98	33.11	-21.20	-24.23	2457821.57-2457825.39	8.708×10^{-3}
NGC4696	192.21	-41.31	35.48	-21.47	-25.61	2457821.57-2457825.39	7.815×10^{-3}
IC3253	185.94	-34.62	34.67	-21.00	-23.59	2457821.57-2457825.39	7.541×10^{-3}
NGC4105	181.67	-29.76	26.55	-20.32	-24.60	2457821.57-2457825.39	7.295×10^{-3}
IC0764	182.56	-29.74	21.18	-20.13	-21.92	2457821.57-2457825.39	6.613×10^{-3}
NGC4373A	186.41	-39.32	37.33	-20.63	-24.06	2457821.57-2457825.39	5.834×10^{-3}
NGC3585	168.32	-26.75	20.05	-20.77	-24.81	2457821.57-2457825.39	5.682×10^{-3}
ESO380-019	185.51	-35.79	38.02	-20.37	-24.24	2457821.57-2457825.39	5.256×10^{-3}
IC3370	186.90	-39.34	26.79	-20.37	-24.28	2457821.57-2457825.39	5.116×10^{-3}
NGC4304	185.55	-33.48	34.67	-20.24	-23.65	2457821.57-2457825.39	4.928×10^{-3}
ESO321-025	185.43	-39.77	29.38	-20.32	-22.58	2457821.57-2457825.39	4.578×10^{-3}
NGC3459	163.68	-17.04	31.61	-20.25	-22.44	2457821.57-2457825.39	4.299×10^{-3}
NGC5365	209.46	-43.93	32.36	-20.35	-24.63	2457821.57-2457825.39	4.286×10^{-3}
PGC086291	283.00	11.88	38.02	-20.63	-24.07	2457821.57-2457825.39	4.207×10^{-3}
NGC5365A	209.16	-44.01	36.98	-20.27	-24.00	2457821.57-2457825.39	3.973×10^{-3}
NGC5078	199.96	-27.41	27.67	-21.24	-25.09	2457821.57-2457825.39	3.946×10^{-3}
ESO320-026	177.46	-38.78	38.02	-20.92	-24.22	2457821.57-2457825.39	3.820×10^{-3}
NGC5101	200.44	-27.43	24.21	-20.68	-24.76	2457821.57-2457825.39	3.675×10^{-3}
IC2977	178.81	-37.70	39.01	-20.82	-23.84	2457821.57-2457825.39	3.626×10^{-3}
ESO320-030	178.30	-39.13	38.02	-20.25	-23.69	2457821.57-2457825.39	3.508×10^{-3}
NGC5643	218.17	-44.17	18.45	-21.16	-24.16	2457821.57-2457825.39	3.359×10^{-3}
ESO442-026	193.06	-29.84	34.94	-20.71	-24.29	2457821.57-2457825.39	3.129×10^{-3}
NGC5266	205.76	-48.17	38.02	-21.14	-25.42	2457821.57-2457825.39	3.090×10^{-3}
ESO221-012	207.89	-48.08	38.02	-20.10	-21.99	2457821.57-2457825.39	3.084×10^{-3}
ESO221-014	208.03	-48.17	35.81	-20.29	-23.14	2457821.57-2457825.39	3.042×10^{-3}
NGC3169	153.56	3.47	18.45	-20.30	-24.05	2457821.57-2457825.39	2.957×10^{-3}
NGC3742	173.89	-37.96	38.61	-20.57	-24.29	2457821.57-2457825.39	2.919×10^{-3}
NGC4767	193.47	-39.71	32.81	-20.38	-24.36	2457821.57-2457825.39	2.858×10^{-3}
NGC3749	173.97	-38.00	38.02	-20.80	-24.20	2457821.57-2457825.39	2.840×10^{-3}
NGC4947	196.33	-35.34	27.80	-20.32	-23.20	2457821.57-2457825.39	2.775×10^{-3}
ESO380-050	189.59	-35.62	38.02	-20.13	-20.51	2457821.57-2457825.39	2.689×10^{-3}
NGC5061	199.52	-26.84	24.21	-20.82	-24.63	2457821.57-2457825.39	2.530×10^{-3}
NGC3783	174.76	-37.74	38.02	-20.50	-24.25	2457821.57-2457825.39	2.483×10^{-3}
PGC046029	198.58	-46.12	36.98	-20.36	-24.31	2457821.57-2457825.39	2.469×10^{-3}
NGC5266A	205.15	-48.34	38.02	-20.75	-22.20	2457821.57-2457825.39	2.425×10^{-3}
ESO321-016	183.86	-38.14	38.02	-20.15	-21.98	2457821.57-2457825.39	2.386×10^{-3}
ESO221-010	207.74	-49.06	38.02	-20.53	-23.65	2457821.57-2457825.39	2.363×10^{-3}
NGC5063	199.61	-35.35	33.39	-20.35	-23.28	2457821.57-2457825.39	2.313×10^{-3}

Table 6 continued

Table 6 (*continued*)

Name (1)	RA(J2000) (2)	DEC(J2000) (3)	Dist(Mpc) (4)	B(mag) (5)	K(mag) (6)	OBS_WINDOW(JD) (7)	SCORE (8)
IC4444	217.91	-43.42	25.35	-20.22	-23.42	2457821.57-2457825.39	2.270×10^{-3}
NGC3706	172.44	-36.39	38.02	-21.00	-25.00	2457821.57-2457825.39	2.221×10^{-3}
ESO271-022	213.38	-45.41	38.14	-20.89	-23.12	2457821.57-2457825.39	2.180×10^{-3}
IC4214	199.43	-32.10	28.84	-20.59	-24.09	2457821.57-2457825.39	2.170×10^{-3}
NGC6574	272.96	14.98	38.91	-20.99	-24.54	2457821.57-2457825.39	2.094×10^{-3}
NGC3115	151.31	-7.72	10.33	-20.13	-24.19	2457821.57-2457825.39	1.955×10^{-3}
ESO221-020	209.60	-48.48	38.29	-20.15	-23.63	2457821.57-2457825.39	1.948×10^{-3}
ESO269-057	197.52	-46.44	36.98	-20.63	-24.06	2457821.57-2457825.39	1.900×10^{-3}
NGC5688	219.90	-45.02	30.90	-20.59	-24.13	2457821.57-2457825.39	1.860×10^{-3}
ESO320-031	178.53	-39.87	38.18	-20.45	-24.87	2457821.57-2457825.39	1.825×10^{-3}
NGC6570	272.78	14.09	33.42	-20.22	-22.75	2457821.57-2457825.39	1.714×10^{-3}
IC4197	197.02	-23.80	34.10	-20.24	-23.39	2457821.57-2457825.39	1.657×10^{-3}
NGC5188	202.87	-34.79	28.84	-20.20	-23.78	2457821.57-2457825.39	1.616×10^{-3}
ESO221-025	211.90	-48.39	38.93	-20.26	-19.44	2457821.57-2457825.39	1.571×10^{-3}
NGC5219	204.67	-45.86	36.98	-20.40	-22.88	2457821.57-2457825.39	1.469×10^{-3}
ESO221-026	212.10	-47.97	20.31	-20.13	-24.00	2457821.57-2457825.39	1.389×10^{-3}
NGC5483	212.60	-43.32	24.21	-20.22	-23.46	2457821.57-2457825.39	1.381×10^{-3}
NGC3962	178.67	-13.97	35.32	-21.24	-25.07	2457821.57-2457825.39	1.362×10^{-3}
ESO507-032	193.06	-26.30	20.82	-20.22	-22.30	2457821.57-2457825.39	1.346×10^{-3}
NGC3672	171.26	-9.80	23.66	-20.77	-23.60	2457821.57-2457825.39	1.306×10^{-3}
NGC6555	271.96	17.60	33.42	-20.82	-22.79	2457821.57-2457825.39	1.303×10^{-3}
NGC4993	197.45	-23.38	39.99	-20.20	-23.42	2457821.57-2457825.39	1.279×10^{-3}
NGC4444	187.15	-43.26	36.98	-20.63	-23.43	2457821.57-2457825.39	1.269×10^{-3}
ESO386-039	224.11	-37.60	36.98	-20.10	-22.89	2457821.57-2457825.39	1.241×10^{-3}
ESO176-006	224.29	-54.39	38.01	-21.52	-24.43	2457821.57-2457825.39	1.213×10^{-3}
NGC2967	145.51	0.34	29.92	-20.24	-23.50	2457821.57-2457825.39	1.209×10^{-3}
NGC5156	202.18	-48.92	36.98	-20.94	-24.11	2457821.57-2457825.39	1.113×10^{-3}
ESO377-024	168.14	-36.43	38.21	-20.23	-22.95	2457821.57-2457825.39	1.081×10^{-3}
NGC6384	263.10	7.06	25.94	-21.26	-24.54	2457821.57-2457825.39	1.062×10^{-3}
NGC3368	161.69	11.82	10.47	-20.18	-23.78	2457821.57-2457825.39	1.021×10^{-3}
NGC4462	187.34	-23.17	23.12	-20.12	-23.36	2457821.57-2457825.39	9.324×10^{-4}
NGC3338	160.53	13.75	24.43	-20.95	-23.81	2457821.57-2457825.39	9.297×10^{-4}
NGC4976	197.16	-49.51	17.30	-20.90	-24.34	2457821.57-2457825.39	9.070×10^{-4}
IC4351	209.48	-29.32	27.54	-20.80	-24.18	2457821.57-2457825.39	8.962×10^{-4}
ESO385-030	217.33	-33.45	34.33	-20.42	-24.09	2457821.57-2457825.39	8.081×10^{-4}
2MASXJ133706182953185	204.25	-29.87	4.92	-20.26	-23.84	2457821.57-2457825.39	7.861×10^{-4}
NGC4219	184.11	-43.32	20.99	-20.51	-23.52	2457821.57-2457825.39	7.476×10^{-4}
NGC4835	194.53	-46.26	20.14	-20.22	-23.34	2457821.57-2457825.39	7.294×10^{-4}
NGC5494	213.10	-30.64	31.19	-20.19	-23.50	2457821.57-2457825.39	6.711×10^{-4}

Table 6 continued

Table 6 (*continued*)

Name (1)	RA(J2000) (2)	DEC(J2000) (3)	Dist(Mpc) (4)	B(mag) (5)	K(mag) (6)	OBS_WINDOW(JD) (7)	SCORE (8)
PGC054411	228.64	-52.99	19.36	-20.60	-24.25	2457821.57-2457825.39	5.852×10^{-4}
ESO175-005	214.45	-52.83	37.36	-20.38	-20.29	2457821.57-2457825.39	5.068×10^{-4}
NGC5085	200.07	-24.44	24.21	-20.32	-23.00	2457821.57-2457825.39	4.894×10^{-4}
NGC4112	181.79	-40.21	34.67	-20.54	-23.50	2457821.57-2457825.39	4.340×10^{-4}
NGC2992	146.43	-14.33	28.84	-20.39	-23.70	2457821.57-2457825.39	2.813×10^{-4}

Table 7. Galaxies observed after trigger G275697 (with the preliminary bayestar localization map). Table columns provide the galaxy name, coordinates, distance, B and K-band magnitude, observing window and the score from our ranking algorithm. The cumulative score is 0.681.

Name (1)	RA(J2000) (2)	DEC(J2000) (3)	Dist(Mpc) (4)	B(mag) (5)	K(mag) (6)	OBS_WINDOW(JD) (7)	SCORE (8)
NGC3742	173.89	-37.96	38.61	-20.57	-24.29	2457812.34-2457820.41	4.087×10^{-2}
NGC3749	173.97	-38.00	38.02	-20.80	-24.20	2457812.34-2457820.41	3.951×10^{-2}
ESO320-026	177.46	-38.78	38.02	-20.92	-24.22	2457812.34-2457820.41	3.305×10^{-2}
ESO320-004	173.68	-38.25	38.02	-19.46	-21.31	2457812.34-2457820.41	3.203×10^{-2}
ESO320-027	177.60	-38.65	37.64	-19.93	-20.41	2457812.34-2457820.41	3.092×10^{-2}
ESO320-024	177.36	-38.83	38.89	-19.55	-21.80	2457812.34-2457820.41	3.087×10^{-2}
NGC3783	174.76	-37.74	38.02	-20.50	-24.25	2457812.34-2457820.41	2.898×10^{-2}
ESO320-030	178.30	-39.13	38.02	-20.25	-23.69	2457812.34-2457820.41	2.888×10^{-2}
NGC3706	172.44	-36.39	38.02	-21.00	-25.00	2457812.34-2457820.41	2.707×10^{-2}
ESO320-031	178.53	-39.87	38.18	-20.45	-24.87	2457812.34-2457820.41	1.918×10^{-2}
NGC3606	169.06	-33.83	37.68	-20.01	-23.49	2457812.34-2457820.41	1.455×10^{-2}
ESO378-012	174.26	-36.82	37.94	-19.51	-22.62	2457812.34-2457820.41	1.423×10^{-2}
ESO221-004	207.47	-48.58	37.96	-19.41	-19.63	2457812.34-2457820.41	1.383×10^{-2}
ESO377-029	168.66	-33.91	38.56	-19.75	-23.41	2457812.34-2457820.41	1.320×10^{-2}
ESO378-020	176.82	-37.55	39.46	-19.90	-23.44	2457812.34-2457820.41	1.240×10^{-2}
ESO221-003	207.44	-48.75	38.02	-19.49	-21.96	2457812.34-2457820.41	1.211×10^{-2}
NGC5266	205.76	-48.17	38.02	-21.14	-25.42	2457812.34-2457820.41	1.210×10^{-2}
NGC3903	177.26	-37.52	38.02	-19.89	-22.63	2457812.34-2457820.41	1.205×10^{-2}
PGC049119	207.62	-48.28	38.02	-20.06	-22.40	2457812.34-2457820.41	1.121×10^{-2}
ESO377-024	168.14	-36.43	38.21	-20.23	-22.95	2457812.34-2457820.41	1.119×10^{-2}
NGC5266A	205.15	-48.34	38.02	-20.75	-22.20	2457812.34-2457820.41	1.119×10^{-2}
ESO221-010	207.74	-49.06	38.02	-20.53	-23.65	2457812.34-2457820.41	1.118×10^{-2}
NGC4976	197.16	-49.51	17.30	-20.90	-24.34	2457812.34-2457820.41	1.118×10^{-2}
NGC3573	167.83	-36.88	37.18	-19.87	-24.02	2457812.34-2457820.41	1.070×10^{-2}
ESO220-026	204.94	-48.30	38.75	-19.41	-19.80	2457812.34-2457820.41	1.040×10^{-2}

Table 7 continued

Table 7 (*continued*)

Name (1)	RA(J2000) (2)	DEC(J2000) (3)	Dist(Mpc) (4)	B(mag) (5)	K(mag) (6)	OBS_WINDOW(JD) (7)	SCORE (8)
NGC5156	202.18	-48.92	36.98	-20.94	-24.11	2457812.34-2457820.41	1.037×10^{-2}
IC2977	178.81	-37.70	39.01	-20.82	-23.84	2457812.34-2457820.41	1.005×10^{-2}
NGC4219	184.11	-43.32	20.99	-20.51	-23.52	2457812.34-2457820.41	9.649×10^{-3}
ESO219-022	195.60	-49.47	23.56	-19.68	-21.99	2457812.34-2457820.41	9.184×10^{-3}
ESO221-014	208.03	-48.17	35.81	-20.29	-23.14	2457812.34-2457820.41	9.143×10^{-3}
ESO377-021	167.74	-35.98	32.81	-19.45	-22.20	2457812.34-2457820.41	9.138×10^{-3}
ESO221-012	207.89	-48.08	38.02	-20.10	-21.99	2457812.34-2457820.41	8.879×10^{-3}
IC3896A	193.88	-50.07	27.67	-20.00	-20.30	2457812.34-2457820.41	8.153×10^{-3}
NGC4444	187.15	-43.26	36.98	-20.63	-23.43	2457812.34-2457820.41	8.134×10^{-3}
ESO269-057	197.52	-46.44	36.98	-20.63	-24.06	2457812.34-2457820.41	7.846×10^{-3}
IC3896	194.18	-50.35	27.67	-20.51	-24.42	2457812.34-2457820.41	7.778×10^{-3}
ESO220-009	201.72	-48.16	37.46	-19.43	-22.70	2457812.34-2457820.41	7.578×10^{-3}
PGC046029	198.58	-46.12	36.98	-20.36	-24.31	2457812.34-2457820.41	6.891×10^{-3}
ESO269-090	200.21	-47.22	37.03	-19.96	-23.35	2457812.34-2457820.41	6.747×10^{-3}
ESO269-085	200.00	-47.28	28.31	-19.46	-23.30	2457812.34-2457820.41	6.448×10^{-3}
ESO221-020	209.60	-48.48	38.29	-20.15	-23.63	2457812.34-2457820.41	5.942×10^{-3}
ESO377-019	167.69	-35.35	37.40	-19.43	-21.72	2457812.34-2457820.41	5.848×10^{-3}
NGC4835	194.53	-46.26	20.14	-20.22	-23.34	2457812.34-2457820.41	4.894×10^{-3}
ESO220-023	204.33	-49.75	38.02	-19.76	-23.23	2457812.34-2457820.41	3.982×10^{-3}
NGC3115	151.31	-7.72	10.33	-20.13	-24.19	2457812.34-2457820.41	3.759×10^{-3}
ESO321-021	185.07	-40.39	39.65	-20.07	-22.64	2457812.34-2457820.41	3.570×10^{-3}
NGC4573	189.43	-43.62	37.42	-19.63	-23.22	2457812.34-2457820.41	3.532×10^{-3}
ESO175-005	214.45	-52.83	37.36	-20.38	-20.29	2457812.34-2457820.41	3.510×10^{-3}
ESO268-027	189.63	-42.86	38.42	-19.37	-22.45	2457812.34-2457820.41	3.454×10^{-3}
ESO319-016	170.53	-38.07	38.22	-19.68	-20.96	2457812.34-2457820.41	3.159×10^{-3}
NGC2967	145.51	0.34	29.92	-20.24	-23.50	2457812.34-2457820.41	2.765×10^{-3}
ESO267-016	181.59	-44.45	39.26	-19.36	-22.30	2457812.34-2457820.41	2.637×10^{-3}
ESO221-032	213.04	-49.39	36.98	-19.87	-23.86	2457812.34-2457820.41	2.309×10^{-3}
ESO321-005	181.45	-38.85	36.46	-19.75	-22.20	2457812.34-2457820.41	2.237×10^{-3}
NGC2974	145.64	-3.70	21.48	-20.01	-25.41	2457812.34-2457820.41	2.202×10^{-3}
ESO438-005	167.24	-28.37	26.18	-19.38	-19.64	2457812.34-2457820.41	2.110×10^{-3}
ESO268-044	192.18	-45.01	37.67	-19.35	-22.26	2457812.34-2457820.41	2.056×10^{-3}
PGC166337	216.65	-52.73	38.39	-19.57	-22.29	2457812.34-2457820.41	2.045×10^{-3}
NGC4112	181.79	-40.21	34.67	-20.54	-23.50	2457812.34-2457820.41	1.912×10^{-3}

Table 8. Galaxies observed after trigger G275697 (with the updated LALInference localization map). Table columns provide the galaxy name, coordinates, distance, B and K-band magnitude, observing window and the score from our ranking algorithm. The cumulative score is 0.574.

Name (1)	RA(J2000) (2)	DEC(J2000) (3)	Dist(Mpc) (4)	B(mag) (5)	K(mag) (6)	OBS_WINDOW(JD) (7)	SCORE (8)
NGC3742	173.89	-37.96	38.61	-20.57	-24.29	2457820.41-2457825.39	1.823×10^{-2}
NGC3749	173.97	-38.00	38.02	-20.80	-24.20	2457820.41-2457825.39	1.761×10^{-2}
NGC3557B	167.38	-37.35	36.98	-20.06	-23.75	2457820.41-2457825.39	1.554×10^{-2}
NGC3573	167.83	-36.88	37.18	-19.87	-24.02	2457820.41-2457825.39	1.538×10^{-2}
ESO320-004	173.68	-38.25	38.02	-19.46	-21.31	2457820.41-2457825.39	1.495×10^{-2}
ESO320-026	177.46	-38.78	38.02	-20.92	-24.22	2457820.41-2457825.39	1.454×10^{-2}
NGC3564	167.65	-37.55	36.98	-20.08	-23.89	2457820.41-2457825.39	1.409×10^{-2}
ESO320-027	177.60	-38.65	37.64	-19.93	-20.41	2457820.41-2457825.39	1.399×10^{-2}
ESO320-024	177.36	-38.83	38.89	-19.55	-21.80	2457820.41-2457825.39	1.348×10^{-2}
NGC3533	166.78	-37.17	36.88	-20.39	-23.59	2457820.41-2457825.39	1.345×10^{-2}
ESO320-030	178.30	-39.13	38.02	-20.25	-23.69	2457820.41-2457825.39	1.293×10^{-2}
ESO377-024	168.14	-36.43	38.21	-20.23	-22.95	2457820.41-2457825.39	1.241×10^{-2}
NGC3783	174.76	-37.74	38.02	-20.50	-24.25	2457820.41-2457825.39	1.211×10^{-2}
NGC3706	172.44	-36.39	38.02	-21.00	-25.00	2457820.41-2457825.39	1.152×10^{-2}
ESO377-010	166.63	-37.65	36.98	-20.37	-23.82	2457820.41-2457825.39	1.142×10^{-2}
ESO377-021	167.74	-35.98	32.81	-19.45	-22.20	2457820.41-2457825.39	9.741×10^{-3}
ESO320-031	178.53	-39.87	38.18	-20.45	-24.87	2457820.41-2457825.39	8.197×10^{-3}
ESO221-004	207.47	-48.58	37.96	-19.41	-19.63	2457820.41-2457825.39	8.051×10^{-3}
PGC049119	207.62	-48.28	38.02	-20.06	-22.40	2457820.41-2457825.39	7.170×10^{-3}
NGC5266	205.76	-48.17	38.02	-21.14	-25.42	2457820.41-2457825.39	7.125×10^{-3}
IC2977	178.81	-37.70	39.01	-20.82	-23.84	2457820.41-2457825.39	7.118×10^{-3}
ESO437-033	159.99	-30.19	36.98	-19.39	-22.91	2457820.41-2457825.39	6.960×10^{-3}
ESO221-003	207.44	-48.75	38.02	-19.49	-21.96	2457820.41-2457825.39	6.813×10^{-3}
NGC3903	177.26	-37.52	38.02	-19.89	-22.63	2457820.41-2457825.39	6.536×10^{-3}
NGC3606	169.06	-33.83	37.68	-20.01	-23.49	2457820.41-2457825.39	6.447×10^{-3}
ESO437-030	159.81	-30.30	39.81	-20.54	-23.69	2457820.41-2457825.39	6.402×10^{-3}
NGC5266A	205.15	-48.34	38.02	-20.75	-22.20	2457820.41-2457825.39	6.342×10^{-3}
NGC4976	197.16	-49.51	17.30	-20.90	-24.34	2457820.41-2457825.39	6.313×10^{-3}
ESO377-029	168.66	-33.91	38.56	-19.75	-23.41	2457820.41-2457825.39	6.272×10^{-3}
ESO221-014	208.03	-48.17	35.81	-20.29	-23.14	2457820.41-2457825.39	6.121×10^{-3}
ESO221-012	207.89	-48.08	38.02	-20.10	-21.99	2457820.41-2457825.39	6.086×10^{-3}
IC3896	194.18	-50.35	27.67	-20.51	-24.42	2457820.41-2457825.39	6.075×10^{-3}
ESO221-010	207.74	-49.06	38.02	-20.53	-23.65	2457820.41-2457825.39	6.065×10^{-3}
IC3896A	193.88	-50.07	27.67	-20.00	-20.30	2457820.41-2457825.39	6.064×10^{-3}
ESO378-020	176.82	-37.55	39.46	-19.90	-23.44	2457820.41-2457825.39	6.060×10^{-3}
NGC5333	208.60	-48.51	35.81	-19.29	-24.40	2457820.41-2457825.39	5.944×10^{-3}
ESO220-026	204.94	-48.30	38.75	-19.41	-19.80	2457820.41-2457825.39	5.909×10^{-3}

Table 8 continued

Table 8 (*continued*)

Name (1)	RA(J2000) (2)	DEC(J2000) (3)	Dist(Mpc) (4)	B(mag) (5)	K(mag) (6)	OBS_WINDOW(JD) (7)	SCORE (8)
ESO378-012	174.26	-36.82	37.94	-19.51	-22.62	2457820.41-2457825.39	5.898×10^{-3}
NGC4603	190.23	-40.98	33.11	-21.20	-24.23	2457820.41-2457825.39	5.590×10^{-3}
ESO176-006	224.29	-54.39	38.01	-21.52	-24.43	2457820.41-2457825.39	5.447×10^{-3}
ESO219-022	195.60	-49.47	23.56	-19.68	-21.99	2457820.41-2457825.39	5.430×10^{-3}
ESO377-019	167.69	-35.35	37.40	-19.43	-21.72	2457820.41-2457825.39	5.276×10^{-3}
NGC4645	191.04	-41.75	29.92	-20.08	-23.94	2457820.41-2457825.39	5.259×10^{-3}
NGC5156	202.18	-48.92	36.98	-20.94	-24.11	2457820.41-2457825.39	5.217×10^{-3}
NGC4603C	190.18	-40.76	38.83	-19.60	-23.11	2457820.41-2457825.39	5.217×10^{-3}
NGC4603A	189.90	-40.74	30.34	-19.45	-22.33	2457820.41-2457825.39	4.926×10^{-3}
ESO269-060	197.75	-46.22	36.98	-19.28	-22.71	2457820.41-2457825.39	4.822×10^{-3}
ESO269-057	197.52	-46.44	36.98	-20.63	-24.06	2457820.41-2457825.39	4.668×10^{-3}
PGC046029	198.58	-46.12	36.98	-20.36	-24.31	2457820.41-2457825.39	4.650×10^{-3}
ESO321-025	185.43	-39.77	29.38	-20.32	-22.58	2457820.41-2457825.39	4.503×10^{-3}
NGC4444	187.15	-43.26	36.98	-20.63	-23.43	2457820.41-2457825.39	4.350×10^{-3}
NGC4219	184.11	-43.32	20.99	-20.51	-23.52	2457820.41-2457825.39	4.316×10^{-3}
NGC4696	192.21	-41.31	35.48	-21.47	-25.61	2457820.41-2457825.39	4.266×10^{-3}
ESO322-045	190.01	-42.04	38.93	-19.98	-23.00	2457820.41-2457825.39	4.182×10^{-3}
ESO221-020	209.60	-48.48	38.29	-20.15	-23.63	2457820.41-2457825.39	4.012×10^{-3}
NGC4373A	186.41	-39.32	37.33	-20.63	-24.06	2457820.41-2457825.39	3.995×10^{-3}
NGC4575	189.46	-40.54	29.11	-19.83	-22.97	2457820.41-2457825.39	3.941×10^{-3}
ESO220-009	201.72	-48.16	37.46	-19.43	-22.70	2457820.41-2457825.39	3.927×10^{-3}
PGC027810	145.82	-9.95	38.39	-20.05	-22.28	2457820.41-2457825.39	3.883×10^{-3}
ESO269-090	200.21	-47.22	37.03	-19.96	-23.35	2457820.41-2457825.39	3.813×10^{-3}
NGC3585	168.32	-26.75	20.05	-20.77	-24.81	2457820.41-2457825.39	3.801×10^{-3}
ESO269-085	200.00	-47.28	28.31	-19.46	-23.30	2457820.41-2457825.39	3.639×10^{-3}
ESO321-021	185.07	-40.39	39.65	-20.07	-22.64	2457820.41-2457825.39	3.638×10^{-3}
ESO269-078	199.16	-45.89	37.86	-19.27	-20.24	2457820.41-2457825.39	3.477×10^{-3}
ESO221-022	210.05	-48.27	34.20	-19.30	-22.60	2457820.41-2457825.39	3.425×10^{-3}
ESO322-042	189.67	-42.21	34.83	-19.61	-21.43	2457820.41-2457825.39	3.384×10^{-3}
NGC2979	145.79	-10.38	38.02	-19.52	-23.39	2457820.41-2457825.39	3.232×10^{-3}
IC3370	186.90	-39.34	26.79	-20.37	-24.28	2457820.41-2457825.39	3.112×10^{-3}
ESO221-025	211.90	-48.39	38.93	-20.26	-19.44	2457820.41-2457825.39	2.954×10^{-3}
PGC028308	147.56	-12.06	38.02	-20.07	-22.58	2457820.41-2457825.39	2.924×10^{-3}
ESO322-027	188.68	-40.30	39.54	-20.03	-23.26	2457820.41-2457825.39	2.886×10^{-3}
ESO319-016	170.53	-38.07	38.22	-19.68	-20.96	2457820.41-2457825.39	2.866×10^{-3}
ESO268-027	189.63	-42.86	38.42	-19.37	-22.45	2457820.41-2457825.39	2.850×10^{-3}
ESO437-014	159.22	-32.35	37.33	-20.16	-23.62	2457820.41-2457825.39	2.668×10^{-3}
NGC4835	194.53	-46.26	20.14	-20.22	-23.34	2457820.41-2457825.39	2.576×10^{-3}
ESO175-005	214.45	-52.83	37.36	-20.38	-20.29	2457820.41-2457825.39	2.427×10^{-3}

Table 8 continued

Table 8 (*continued*)

Name (1)	RA(J2000) (2)	DEC(J2000) (3)	Dist(Mpc) (4)	B(mag) (5)	K(mag) (6)	OBS_WINDOW(JD) (7)	SCORE (8)
ESO221-026	212.10	-47.97	20.31	-20.13	-24.00	2457820.41-2457825.39	2.364×10^{-3}
NGC3208	154.92	-25.81	36.98	-19.63	-23.43	2457820.41-2457825.39	2.336×10^{-3}
NGC3203	154.89	-26.70	32.36	-19.99	-23.69	2457820.41-2457825.39	2.250×10^{-3}
NGC4573	189.43	-43.62	37.42	-19.63	-23.22	2457820.41-2457825.39	2.239×10^{-3}
ESO376-009	160.51	-33.25	38.78	-19.67	-23.40	2457820.41-2457825.39	2.084×10^{-3}
ESO321-010	182.93	-38.55	38.02	-19.66	-22.79	2457820.41-2457825.39	2.075×10^{-3}
ESO321-019	184.27	-39.05	37.64	-19.77	-22.82	2457820.41-2457825.39	2.071×10^{-3}
PGC054411	228.64	-52.99	19.36	-20.60	-24.25	2457820.41-2457825.39	2.049×10^{-3}
ESO220-023	204.33	-49.75	38.02	-19.76	-23.23	2457820.41-2457825.39	2.033×10^{-3}
NGC2974	145.64	-3.70	21.48	-20.01	-25.41	2457820.41-2457825.39	1.974×10^{-3}
ESO270-006	200.49	-45.94	36.98	-19.95	-22.57	2457820.41-2457825.39	1.957×10^{-3}
ESO321-005	181.45	-38.85	36.46	-19.75	-22.20	2457820.41-2457825.39	1.935×10^{-3}
NGC3115	151.31	-7.72	10.33	-20.13	-24.19	2457820.41-2457825.39	1.896×10^{-3}
NGC3717	172.88	-30.31	16.90	-19.94	-23.62	2457820.41-2457825.39	1.842×10^{-3}
ESO321-016	183.86	-38.14	38.02	-20.15	-21.98	2457820.41-2457825.39	1.728×10^{-3}
ESO322-020	187.30	-40.69	39.58	-19.39	-20.47	2457820.41-2457825.39	1.660×10^{-3}
NGC2967	145.51	0.34	29.92	-20.24	-23.50	2457820.41-2457825.39	1.637×10^{-3}
ESO267-016	181.59	-44.45	39.26	-19.36	-22.30	2457820.41-2457825.39	1.623×10^{-3}
NGC5219	204.67	-45.86	36.98	-20.40	-22.88	2457820.41-2457825.39	1.547×10^{-3}
ESO321-018	183.98	-38.09	38.65	-19.78	-19.60	2457820.41-2457825.39	1.450×10^{-3}
PGC166337	216.65	-52.73	38.39	-19.57	-22.29	2457820.41-2457825.39	1.400×10^{-3}
ESO221-032	213.04	-49.39	36.98	-19.87	-23.86	2457820.41-2457825.39	1.395×10^{-3}
ESO438-005	167.24	-28.37	26.18	-19.38	-19.64	2457820.41-2457825.39	1.264×10^{-3}
PGC166343	219.26	-54.04	38.04	-19.70	-21.29	2457820.41-2457825.39	1.197×10^{-3}
ESO268-044	192.18	-45.01	37.67	-19.35	-22.26	2457820.41-2457825.39	1.175×10^{-3}
NGC4112	181.79	-40.21	34.67	-20.54	-23.50	2457820.41-2457825.39	1.126×10^{-3}
NGC4751	193.21	-42.66	26.19	-19.67	-23.86	2457820.41-2457825.39	1.102×10^{-3}
ESO175-009	218.00	-55.47	39.26	-19.60	-24.01	2457820.41-2457825.39	1.070×10^{-3}
NGC2775	137.58	7.04	17.30	-20.17	-24.15	2457820.41-2457825.39	1.053×10^{-3}
IC2580	157.08	-31.52	36.98	-19.70	-22.80	2457820.41-2457825.39	1.036×10^{-3}
NGC3511	165.85	-23.09	12.25	-19.64	-22.37	2457820.41-2457825.39	1.006×10^{-3}
NGC2993	146.45	-14.37	28.84	-19.48	-22.17	2457820.41-2457825.39	9.519×10^{-4}
NGC2992	146.43	-14.33	28.84	-20.39	-23.70	2457820.41-2457825.39	9.074×10^{-4}
IC2627	167.47	-23.73	24.21	-19.62	-22.93	2457820.41-2457825.39	8.357×10^{-4}
ESO569-014	162.85	-19.89	24.77	-19.33	-20.98	2457820.41-2457825.39	7.522×10^{-4}
NGC3175	153.68	-28.87	13.87	-19.39	-22.92	2457820.41-2457825.39	7.353×10^{-4}
ESO222-015	221.12	-49.40	29.92	-19.41	-18.95	2457820.41-2457825.39	6.982×10^{-4}
NGC2947	144.02	-12.44	39.88	-19.37	-23.05	2457820.41-2457825.39	6.017×10^{-4}

Table 9. Galaxies observed after trigger G277583. Table columns provide the galaxy name, coordinates, distance, B and K-band magnitude, observing window and the score from our ranking algorithm. The cumulative score is 0.370.

Name (1)	RA(J2000) (2)	DEC(J2000) (3)	Dist(Mpc) (4)	B(mag) (5)	K(mag) (6)	OBS_WINDOW(JD) (7)	SCORE (8)
NGC1407	55.05	-18.58	28.84	-21.65	-25.60	2457826.53-2457847.24	1.595×10^{-2}
NGC1400	54.88	-18.69	26.42	-20.17	-24.30	2457826.53-2457847.24	1.502×10^{-2}
NGC1393	54.66	-18.43	23.89	-19.49	-22.71	2457826.53-2457847.24	1.293×10^{-2}
NGC1421	55.62	-13.49	25.35	-21.11	-23.62	2457826.53-2457847.24	1.102×10^{-2}
NGC1625	69.28	-3.30	36.98	-20.44	-20.41	2457826.53-2457847.24	8.936×10^{-3}
PGC013646	55.73	-12.92	25.35	-19.62	-22.63	2457826.53-2457847.24	8.625×10^{-3}
IC2098	72.68	-5.42	32.36	-19.77	-22.35	2457826.53-2457847.24	8.333×10^{-3}
NGC1665	72.07	-5.43	33.10	-19.32	-23.34	2457826.53-2457847.24	6.994×10^{-3}
NGC1681	72.96	-5.80	32.36	-19.20	-22.15	2457826.53-2457847.24	6.709×10^{-3}
NGC1398	54.72	-26.34	24.77	-21.50	-25.47	2457826.53-2457847.24	6.696×10^{-3}
NGC1387	54.24	-35.51	20.32	-19.54	-24.11	2457826.53-2457847.24	6.453×10^{-3}
NGC1399	54.62	-35.45	19.95	-20.65	-25.19	2457826.53-2457847.24	6.184×10^{-3}
NGC1389	54.30	-35.75	21.68	-19.29	-23.05	2457826.53-2457847.24	6.155×10^{-3}
NGC1379	54.02	-35.44	20.05	-19.44	-23.27	2457826.53-2457847.24	6.142×10^{-3}
NGC2339	107.09	18.78	37.84	-21.21	-24.38	2457826.53-2457847.24	6.076×10^{-3}
NGC1404	54.72	-35.59	20.99	-20.41	-24.79	2457826.53-2457847.24	5.940×10^{-3}
NGC1395	54.62	-23.03	24.10	-20.75	-25.02	2457826.53-2457847.24	5.370×10^{-3}
NGC1380	54.11	-34.98	17.62	-20.13	-24.36	2457826.53-2457847.24	4.995×10^{-3}
NGC6118	245.45	-2.28	20.99	-20.21	-22.91	2457826.53-2457847.24	4.859×10^{-3}
NGC1784	76.36	-11.87	30.48	-20.50	-23.91	2457826.53-2457847.24	4.672×10^{-3}
NGC1426	55.70	-22.11	24.10	-19.63	-23.24	2457826.53-2457847.24	4.664×10^{-3}
NGC1666	72.14	-6.57	33.08	-19.63	-23.16	2457826.53-2457847.24	4.655×10^{-3}
PGC016894	77.92	-14.79	27.42	-20.19	-22.00	2457826.53-2457847.24	4.305×10^{-3}
NGC1332	51.57	-21.34	22.91	-20.63	-24.75	2457826.53-2457847.24	4.238×10^{-3}
NGC1365	53.40	-36.14	17.95	-21.39	-24.90	2457826.53-2457847.24	4.218×10^{-3}
PGC013716	56.00	-14.36	16.54	-19.22	-21.18	2457826.53-2457847.24	4.203×10^{-3}
NGC1439	56.21	-21.92	26.67	-19.61	-23.56	2457826.53-2457847.24	3.870×10^{-3}
UGC10288	243.60	-0.21	32.96	-19.99	-23.20	2457826.53-2457847.24	3.857×10^{-3}
NGC1359	53.45	-19.49	38.91	-20.57	-21.78	2457826.53-2457847.24	3.801×10^{-3}
NGC1325	51.11	-21.54	19.95	-19.72	-22.87	2457826.53-2457847.24	3.574×10^{-3}
NGC1832	78.01	-15.69	25.12	-20.32	-23.61	2457826.53-2457847.24	3.294×10^{-3}
NGC1427	55.58	-35.39	23.55	-19.92	-23.72	2457826.53-2457847.24	3.250×10^{-3}
PGC016917	78.10	-14.36	29.78	-19.36	-20.51	2457826.53-2457847.24	3.248×10^{-3}
UGC03258	77.68	0.41	35.13	-19.59	-22.37	2457826.53-2457847.24	3.063×10^{-3}
NGC1888	80.64	-11.50	28.84	-20.40	-23.99	2457826.53-2457847.24	2.896×10^{-3}
NGC6063	241.80	7.98	37.50	-19.48	-22.32	2457826.53-2457847.24	2.882×10^{-3}
NGC4373A	186.41	-39.32	37.33	-20.63	-24.06	2457826.53-2457847.24	2.795×10^{-3}
ESO380-006	183.89	-35.63	38.93	-21.31	-24.79	2457826.53-2457847.24	2.739×10^{-3}

Table 9 continued

Table 9 (*continued*)

Name (1)	RA(J2000) (2)	DEC(J2000) (3)	Dist(Mpc) (4)	B(mag) (5)	K(mag) (6)	OBS_WINDOW(JD) (7)	SCORE (8)
NGC1954	83.20	-14.06	38.02	-20.93	-23.80	2457826.53-2457847.24	2.636×10^{-3}
UGC03587	103.48	19.30	23.99	-19.70	-21.31	2457826.53-2457847.24	2.569×10^{-3}
NGC5962	234.13	16.61	30.20	-20.55	-23.87	2457826.53-2457847.24	2.492×10^{-3}
ESO321-025	185.43	-39.77	29.38	-20.32	-22.58	2457826.53-2457847.24	2.469×10^{-3}
IC3370	186.90	-39.34	26.79	-20.37	-24.28	2457826.53-2457847.24	2.402×10^{-3}
NGC6106	244.70	7.41	24.66	-19.60	-22.34	2457826.53-2457847.24	2.400×10^{-3}
NGC6014	238.99	5.93	31.19	-19.42	-22.67	2457826.53-2457847.24	2.386×10^{-3}
NGC1297	49.81	-19.10	28.58	-19.68	-23.35	2457826.53-2457847.24	2.344×10^{-3}
NGC1300	49.92	-19.41	14.52	-19.86	-23.25	2457826.53-2457847.24	2.291×10^{-3}
NGC1353	53.01	-20.82	17.30	-19.36	-23.08	2457826.53-2457847.24	2.272×10^{-3}
IC2977	178.81	-37.70	39.01	-20.82	-23.84	2457826.53-2457847.24	2.268×10^{-3}
NGC1532	63.02	-32.87	17.30	-20.54	-24.46	2457826.53-2457847.24	2.197×10^{-3}
NGC5970	234.62	12.19	26.06	-20.13	-23.26	2457826.53-2457847.24	2.195×10^{-3}
ESO322-027	188.68	-40.30	39.54	-20.03	-23.26	2457826.53-2457847.24	2.058×10^{-3}
NGC1436	55.90	-35.85	19.86	-19.30	-22.46	2457826.53-2457847.24	2.048×10^{-3}
NGC1357	53.32	-13.66	25.35	-19.68	-23.60	2457826.53-2457847.24	2.030×10^{-3}
IC0407	79.43	-15.52	35.81	-20.24	-22.86	2457826.53-2457847.24	2.021×10^{-3}
ESO321-016	183.86	-38.14	38.02	-20.15	-21.98	2457826.53-2457847.24	2.004×10^{-3}
NGC1537	63.42	-31.65	23.23	-20.21	-24.10	2457826.53-2457847.24	1.965×10^{-3}
ESO321-018	183.98	-38.09	38.65	-19.78	-19.60	2457826.53-2457847.24	1.957×10^{-3}
NGC1367	53.76	-24.93	17.30	-19.76	-23.56	2457826.53-2457847.24	1.949×10^{-3}
NGC6012	238.56	14.60	25.83	-19.76	-22.52	2457826.53-2457847.24	1.903×10^{-3}
NGC1924	82.01	-5.31	28.84	-19.83	-22.96	2457826.53-2457847.24	1.882×10^{-3}
ESO320-035	179.19	-38.19	27.04	-19.22	-21.87	2457826.53-2457847.24	1.875×10^{-3}
NGC6181	248.09	19.83	33.57	-20.73	-23.96	2457826.53-2457847.24	1.833×10^{-3}
ESO320-031	178.53	-39.87	38.18	-20.45	-24.87	2457826.53-2457847.24	1.791×10^{-3}
NGC4444	187.15	-43.26	36.98	-20.63	-23.43	2457826.53-2457847.24	1.764×10^{-3}
NGC1232	47.44	-20.58	14.52	-20.42	-23.43	2457826.53-2457847.24	1.756×10^{-3}
ESO321-021	185.07	-40.39	39.65	-20.07	-22.64	2457826.53-2457847.24	1.667×10^{-3}
NGC1425	55.55	-29.89	21.88	-20.36	-23.39	2457826.53-2457847.24	1.659×10^{-3}
NGC1302	49.96	-26.06	19.59	-20.06	-23.63	2457826.53-2457847.24	1.646×10^{-3}
ESO321-019	184.27	-39.05	37.64	-19.77	-22.82	2457826.53-2457847.24	1.638×10^{-3}
NGC1309	50.53	-15.40	23.12	-19.92	-22.72	2457826.53-2457847.24	1.612×10^{-3}
NGC6923	307.91	-30.83	37.15	-20.51	-24.04	2457826.53-2457847.24	1.604×10^{-3}
NGC5956	233.74	11.75	26.28	-19.37	-22.23	2457826.53-2457847.24	1.601×10^{-3}
NGC6010	238.58	0.54	25.35	-19.91	-23.09	2457826.53-2457847.24	1.589×10^{-3}
ESO380-019	185.51	-35.79	38.02	-20.37	-24.24	2457826.53-2457847.24	1.538×10^{-3}
NGC4219	184.11	-43.32	20.99	-20.51	-23.52	2457826.53-2457847.24	1.492×10^{-3}
NGC1340	52.08	-31.07	19.77	-20.23	-24.08	2457826.53-2457847.24	1.481×10^{-3}

Table 9 continued

Table 9 (*continued*)

Name (1)	RA(J2000) (2)	DEC(J2000) (3)	Dist(Mpc) (4)	B(mag) (5)	K(mag) (6)	OBS_WINDOW(JD) (7)	SCORE (8)
ESO321-010	182.93	-38.55	38.02	-19.66	-22.79	2457826.53-2457847.24	1.474×10^{-3}
ESO268-027	189.63	-42.86	38.42	-19.37	-22.45	2457826.53-2457847.24	1.367×10^{-3}
NGC1354	53.12	-15.22	20.75	-19.20	-22.66	2457826.53-2457847.24	1.309×10^{-3}
IC1151	239.63	17.44	24.21	-19.38	-21.51	2457826.53-2457847.24	1.257×10^{-3}
IC5007	310.89	-29.70	32.66	-19.94	-22.46	2457826.53-2457847.24	1.256×10^{-3}
NGC5951	233.43	15.01	25.94	-19.37	-22.02	2457826.53-2457847.24	1.207×10^{-3}
NGC1843	78.53	-10.63	29.92	-19.22	-22.67	2457826.53-2457847.24	1.204×10^{-3}
IC5039	310.81	-29.85	29.51	-19.85	-22.44	2457826.53-2457847.24	1.202×10^{-3}
UGC03691	107.01	15.18	28.84	-20.00	-21.99	2457826.53-2457847.24	1.139×10^{-3}
PGC012664	50.73	-11.20	34.67	-19.73	-21.10	2457826.53-2457847.24	1.018×10^{-3}
ESO460-026	295.75	-27.42	18.11	-19.38	-21.96	2457826.53-2457847.24	9.656×10^{-4}
NGC1350	52.78	-33.63	16.67	-19.95	-23.71	2457826.53-2457847.24	9.590×10^{-4}
UGC10041	237.26	5.19	35.81	-19.27	-19.43	2457826.53-2457847.24	9.588×10^{-4}
ESO322-020	187.30	-40.69	39.58	-19.39	-20.47	2457826.53-2457847.24	9.454×10^{-4}
NGC4573	189.43	-43.62	37.42	-19.63	-23.22	2457826.53-2457847.24	8.463×10^{-4}
NGC1289	49.71	-1.97	35.40	-19.89	-23.25	2457826.53-2457847.24	8.431×10^{-4}
NGC1338	52.23	-12.15	32.36	-19.18	-22.54	2457826.53-2457847.24	7.990×10^{-4}
NGC1406	54.85	-31.32	17.78	-19.35	-22.64	2457826.53-2457847.24	7.880×10^{-4}
NGC1255	48.38	-25.73	17.70	-19.83	-22.86	2457826.53-2457847.24	7.629×10^{-4}
ESO321-005	181.45	-38.85	36.46	-19.75	-22.20	2457826.53-2457847.24	7.583×10^{-4}
UGC09977	235.50	0.71	31.33	-19.48	-21.88	2457826.53-2457847.24	7.198×10^{-4}
ESO595-014	301.91	-21.13	29.92	-19.48	-22.38	2457826.53-2457847.24	6.539×10^{-4}
PGC012633	50.57	-7.09	33.89	-19.24	-22.34	2457826.53-2457847.24	6.168×10^{-4}
PGC017323	82.06	-16.12	25.35	-19.19	-20.84	2457826.53-2457847.24	6.044×10^{-4}
NGC1292	49.56	-27.61	18.97	-19.19	-21.99	2457826.53-2457847.24	5.734×10^{-4}
NGC3882	176.53	-56.39	23.12	-19.47	-23.71	2457826.53-2457847.24	5.256×10^{-4}
ESO267-016	181.59	-44.45	39.26	-19.36	-22.30	2457826.53-2457847.24	5.193×10^{-4}
NGC3149	150.93	-80.42	26.55	-19.49	-22.69	2457826.53-2457847.24	4.971×10^{-4}
IC2006	58.62	-35.97	20.80	-19.32	-23.11	2457826.53-2457847.24	4.943×10^{-4}
UGC03457	95.46	0.37	33.42	-19.66	-24.32	2457826.53-2457847.24	4.911×10^{-4}
ESO019-006	169.05	-79.40	37.43	-19.29	-22.22	2457826.53-2457847.24	4.392×10^{-4}
PGC090034	91.55	-0.54	25.35	-19.33	-22.07	2457826.53-2457847.24	4.061×10^{-4}
ESO554-002	82.28	-19.93	36.21	-19.32	-20.30	2457826.53-2457847.24	3.974×10^{-4}
NGC1179	45.66	-18.90	17.86	-19.26	-19.19	2457826.53-2457847.24	3.950×10^{-4}
NGC4112	181.79	-40.21	34.67	-20.54	-23.50	2457826.53-2457847.24	3.886×10^{-4}

Table 10. Galaxies observed after trigger G284239. Table columns provide the galaxy name, coordinates, distance, B and K-band magnitude, observing window and the score from our ranking algorithm. The cumulative score is 0.846.

Name (1)	RA(J2000) (2)	DEC(J2000) (3)	Dist(Mpc) (4)	B(mag) (5)	K(mag) (6)	OBS_WINDOW(JD) (7)	SCORE (8)
NGC6861	301.83	-48.37	28.05	-20.29	-24.53	2457877.13-2457892.23	6.452×10^{-2}
ESO233-035	302.36	-48.28	33.97	-18.57	-22.23	2457877.13-2457892.23	6.320×10^{-2}
NGC6861D	302.08	-48.21	33.42	-18.90	-23.42	2457877.13-2457892.23	6.280×10^{-2}
NGC6868	302.48	-48.38	26.79	-20.45	-24.82	2457877.13-2457892.23	6.110×10^{-2}
NGC6870	302.55	-48.29	33.42	-19.90	-23.67	2457877.13-2457892.23	6.030×10^{-2}
NGC6861E	302.76	-48.69	33.90	-18.55	-21.04	2457877.13-2457892.23	4.919×10^{-2}
NGC6851	300.89	-48.28	36.14	-20.13	-24.02	2457877.13-2457892.23	4.075×10^{-2}
NGC6384	263.10	7.06	25.94	-21.26	-24.54	2457877.13-2457892.23	2.247×10^{-2}
NGC6887	304.32	-52.80	30.06	-20.49	-23.52	2457877.13-2457892.23	2.239×10^{-2}
NGC7083	323.94	-63.90	29.78	-20.77	-23.95	2457877.13-2457892.23	1.690×10^{-2}
NGC7096	325.33	-63.91	35.81	-20.27	-23.82	2457877.13-2457892.23	1.420×10^{-2}
IC5120	324.70	-64.35	37.33	-19.56	-22.06	2457877.13-2457892.23	1.417×10^{-2}
NGC6889	304.72	-53.96	30.22	-19.49	-22.01	2457877.13-2457892.23	1.258×10^{-2}
IC4837A	288.82	-54.13	33.42	-21.15	-24.47	2457877.13-2457892.23	1.258×10^{-2}
NGC7191	331.72	-64.63	35.83	-19.96	-22.63	2457877.13-2457892.23	1.144×10^{-2}
NGC7192	331.71	-64.32	37.84	-20.68	-24.38	2457877.13-2457892.23	1.119×10^{-2}
IC4837	288.81	-54.67	33.42	-20.72	-20.38	2457877.13-2457892.23	1.088×10^{-2}
NGC7140	328.06	-55.57	35.81	-21.01	-23.82	2457877.13-2457892.23	1.067×10^{-2}
IC4839	288.89	-54.63	35.11	-20.02	-23.48	2457877.13-2457892.23	1.043×10^{-2}
IC4889	296.31	-54.34	29.24	-20.33	-24.22	2457877.13-2457892.23	1.029×10^{-2}
IC4888	296.22	-54.46	29.82	-18.29	-21.26	2457877.13-2457892.23	9.767×10^{-3}
ESO107-015	318.43	-63.34	36.48	-19.20	-22.10	2457877.13-2457892.23	9.251×10^{-3}
NGC7125	327.32	-60.71	36.98	-20.17	-22.63	2457877.13-2457892.23	9.043×10^{-3}
NGC7126	327.33	-60.61	36.98	-19.82	-23.09	2457877.13-2457892.23	8.983×10^{-3}
NGC6909	306.91	-47.03	35.48	-20.04	-23.53	2457877.13-2457892.23	8.959×10^{-3}
NGC7219	333.28	-64.85	36.21	-19.88	-23.02	2457877.13-2457892.23	8.773×10^{-3}
IC5084	317.31	-63.29	36.98	-19.50	-23.59	2457877.13-2457892.23	8.707×10^{-3}
UGC10862	262.04	7.42	25.35	-19.22	-20.32	2457877.13-2457892.23	8.593×10^{-3}
NGC6181	248.09	19.83	33.57	-20.73	-23.96	2457877.13-2457892.23	7.940×10^{-3}
NGC6875A	302.98	-46.14	29.11	-19.52	-22.35	2457877.13-2457892.23	7.841×10^{-3}
IC5092	319.06	-64.46	35.81	-20.17	-23.36	2457877.13-2457892.23	7.216×10^{-3}
NGC6890	304.58	-44.81	31.19	-19.52	-23.44	2457877.13-2457892.23	6.834×10^{-3}
ESO231-017	286.19	-47.85	35.14	-19.62	-23.20	2457877.13-2457892.23	6.820×10^{-3}
NGC6788	291.71	-54.95	34.56	-21.09	-24.17	2457877.13-2457892.23	6.777×10^{-3}
ESO108-023	334.13	-64.39	34.67	-19.33	-20.06	2457877.13-2457892.23	6.520×10^{-3}
NGC7007	316.37	-52.55	34.67	-19.75	-23.74	2457877.13-2457892.23	6.482×10^{-3}
NGC1625	69.28	-3.30	36.98	-20.44	-20.41	2457877.13-2457892.23	6.474×10^{-3}
NGC6368	261.80	11.54	30.48	-20.62	-23.23	2457877.13-2457892.23	6.217×10^{-3}

Table 10 continued

Table 10 (*continued*)

Name (1)	RA(J2000) (2)	DEC(J2000) (3)	Dist(Mpc) (4)	B(mag) (5)	K(mag) (6)	OBS_WINDOW(JD) (7)	SCORE (8)
NGC7029	317.97	-49.28	38.37	-20.23	-24.38	2457877.13-2457892.23	5.843×10^{-3}
ESO234-049	308.83	-49.87	31.19	-19.33	-21.87	2457877.13-2457892.23	5.789×10^{-3}
NGC7041	319.13	-48.36	25.70	-20.06	-23.84	2457877.13-2457892.23	5.719×10^{-3}
ESO235-085	319.57	-48.54	24.03	-18.53	-21.63	2457877.13-2457892.23	5.639×10^{-3}
ESO186-062	308.51	-52.98	31.19	-19.10	-22.22	2457877.13-2457892.23	5.623×10^{-3}
IC4986	304.30	-55.04	23.75	-19.08	-19.92	2457877.13-2457892.23	5.408×10^{-3}
NGC7049	319.74	-48.56	29.92	-20.61	-25.13	2457877.13-2457892.23	5.378×10^{-3}
NGC6810	295.89	-58.66	23.12	-20.42	-24.14	2457877.13-2457892.23	4.947×10^{-3}
IC4821	287.38	-55.02	25.00	-18.98	-21.61	2457877.13-2457892.23	4.568×10^{-3}
NGC7022	317.40	-49.30	29.49	-18.51	-22.12	2457877.13-2457892.23	4.554×10^{-3}
NGC6902B	305.78	-43.87	34.67	-18.69	-20.75	2457877.13-2457892.23	4.340×10^{-3}
NGC7205	332.14	-57.44	17.14	-19.87	-23.25	2457877.13-2457892.23	4.227×10^{-3}
IC4946	305.99	-44.00	34.67	-20.12	-23.97	2457877.13-2457892.23	3.980×10^{-3}
IC4797	284.12	-54.31	28.05	-20.23	-24.17	2457877.13-2457892.23	3.965×10^{-3}
NGC6707	283.84	-53.82	33.42	-18.90	-22.97	2457877.13-2457892.23	3.426×10^{-3}
NGC1665	72.07	-5.43	33.10	-19.32	-23.34	2457877.13-2457892.23	3.165×10^{-3}
ESO183-030	284.23	-54.55	33.42	-20.11	-24.29	2457877.13-2457892.23	3.153×10^{-3}
IC4901	298.60	-58.71	17.86	-19.61	-22.41	2457877.13-2457892.23	3.024×10^{-3}
NGC6990	314.99	-55.56	25.36	-18.57	-21.08	2457877.13-2457892.23	2.858×10^{-3}
UGC11030	268.64	2.88	27.67	-19.06	-19.63	2457877.13-2457892.23	2.152×10^{-3}
IC4817	286.55	-56.16	33.42	-18.96	-21.27	2457877.13-2457892.23	2.013×10^{-3}
NGC7059	321.84	-60.01	20.32	-18.62	-21.93	2457877.13-2457892.23	1.987×10^{-3}
UGC03070	67.75	-2.00	30.65	-18.54	-20.39	2457877.13-2457892.23	1.847×10^{-3}
NGC6509	269.86	6.29	27.67	-19.81	-22.48	2457877.13-2457892.23	1.807×10^{-3}
IC5176	333.73	-66.85	26.42	-19.31	-23.37	2457877.13-2457892.23	1.799×10^{-3}
ESO185-027	299.06	-56.91	23.81	-18.73	-21.94	2457877.13-2457892.23	1.782×10^{-3}
UGC11093	270.47	6.97	21.18	-19.23	-22.25	2457877.13-2457892.23	1.732×10^{-3}
ESO285-048	311.17	-45.98	28.18	-18.77	-21.33	2457877.13-2457892.23	1.670×10^{-3}
ESO236-006	320.29	-47.52	28.93	-18.66	-19.52	2457877.13-2457892.23	1.648×10^{-3}
NGC1637	70.37	-2.86	9.77	-18.54	-21.98	2457877.13-2457892.23	1.618×10^{-3}
IC5249	341.78	-64.83	31.48	-19.52	-19.92	2457877.13-2457892.23	1.546×10^{-3}
ESO235-001	312.26	-47.30	33.75	-18.51	-20.22	2457877.13-2457892.23	1.541×10^{-3}
NGC6149	246.85	19.60	30.57	-18.65	-22.15	2457877.13-2457892.23	1.493×10^{-3}
PGC015873	70.79	0.74	29.92	-18.41	-21.06	2457877.13-2457892.23	1.449×10^{-3}
UGC03258	77.68	0.41	35.13	-19.59	-22.37	2457877.13-2457892.23	1.417×10^{-3}
ESO340-010	304.36	-41.13	39.26	-18.82	-22.12	2457877.13-2457892.23	1.340×10^{-3}
ESO146-001	329.09	-59.29	23.12	-18.28	-20.06	2457877.13-2457892.23	1.256×10^{-3}
ESO340-032	306.73	-39.62	33.54	-18.98	-21.17	2457877.13-2457892.23	1.127×10^{-3}
NGC7090	324.12	-54.56	6.28	-18.56	-20.83	2457877.13-2457892.23	1.097×10^{-3}

Table 10 continued

Table 10 (*continued*)

Name (1)	RA(J2000) (2)	DEC(J2000) (3)	Dist(Mpc) (4)	B(mag) (5)	K(mag) (6)	OBS_WINDOW(JD) (7)	SCORE (8)
PGC061359	271.09	7.28	28.11	-18.50	-23.01	2457877.13-2457892.23	1.041×10^{-3}
IC4871	293.93	-57.52	22.59	-18.80	-20.88	2457877.13-2457892.23	8.689×10^{-4}
PGC016060	72.14	-3.87	33.24	-18.36	-22.35	2457877.13-2457892.23	8.062×10^{-4}
ESO286-063	317.47	-45.53	31.81	-19.21	-21.90	2457877.13-2457892.23	6.683×10^{-4}
IC1151	239.63	17.44	24.21	-19.38	-21.51	2457877.13-2457892.23	5.755×10^{-4}
NGC1507	61.11	-2.20	11.02	-18.41	-20.20	2457877.13-2457892.23	5.466×10^{-4}
UGC02984	63.30	13.42	20.76	-18.55	-19.44	2457877.13-2457892.23	3.196×10^{-4}
IC4885	295.97	-60.65	29.92	-18.39	-21.35	2457877.13-2457892.23	2.645×10^{-4}

Table 11. Galaxies observed after trigger GW170814/G297595. Table columns provide the galaxy name, coordinates, distance, B and K-band magnitude, observing window and the score from our ranking algorithm. The cumulative score is 0.550.

Name (1)	RA(J2000) (2)	DEC(J2000) (3)	Dist(Mpc) (4)	B(mag) (5)	K(mag) (6)	OBS_WINDOW(JD) (7)	SCORE (8)
ESO300-014	47.41	-41.03	10.86	-18.32	-16.32	2457980.28-2457982.25	4.898×10^{-2}
NGC1255	48.38	-25.73	17.70	-19.83	-22.86	2457980.28-2457982.25	4.695×10^{-2}
ESO481-018	49.64	-25.84	18.53	-18.28	-20.64	2457980.28-2457982.25	4.544×10^{-2}
NGC0986	38.39	-39.05	23.12	-20.16	-24.04	2457980.28-2457982.25	4.508×10^{-2}
NGC1201	46.03	-26.07	19.33	-20.01	-23.76	2457980.28-2457982.25	4.045×10^{-2}
NGC1302	49.96	-26.06	19.59	-20.06	-23.63	2457980.28-2457982.25	4.039×10^{-2}
NGC0908	35.77	-21.23	15.78	-20.53	-23.76	2457980.28-2457982.25	2.868×10^{-2}
PGC013359	54.31	1.86	22.59	-19.15	-20.80	2457980.28-2457982.25	2.490×10^{-2}
NGC1097	41.58	-30.27	14.19	-20.74	-24.51	2457980.28-2457982.25	2.430×10^{-2}
NGC1232	47.44	-20.58	14.52	-20.42	-23.43	2457980.28-2457982.25	2.424×10^{-2}
NGC1300	49.92	-19.41	14.52	-19.86	-23.25	2457980.28-2457982.25	2.200×10^{-2}
NGC1292	49.56	-27.61	18.97	-19.19	-21.99	2457980.28-2457982.25	2.177×10^{-2}
NGC1325	51.11	-21.54	19.95	-19.72	-22.87	2457980.28-2457982.25	2.159×10^{-2}
NGC1297	49.81	-19.10	28.58	-19.68	-23.35	2457980.28-2457982.25	2.141×10^{-2}
NGC1187	45.66	-22.87	18.36	-20.03	-23.22	2457980.28-2457982.25	1.612×10^{-2}
IC1892	47.11	-23.06	34.67	-18.85	-19.74	2457980.28-2457982.25	1.418×10^{-2}
ESO545-005	35.03	-19.75	30.20	-19.15	-21.80	2457980.28-2457982.25	1.314×10^{-2}
IC1898	47.58	-22.41	19.50	-18.39	-21.41	2457980.28-2457982.25	1.057×10^{-2}
PGC1075354	52.68	-3.16	24.72	-18.94	-21.05	2457980.28-2457982.25	9.864×10^{-3}
NGC1309	50.53	-15.40	23.12	-19.92	-22.72	2457980.28-2457982.25	9.671×10^{-3}
PGC012664	50.73	-11.20	34.67	-19.73	-21.10	2457980.28-2457982.25	7.206×10^{-3}
PGC012633	50.57	-7.09	33.89	-19.24	-22.34	2457980.28-2457982.25	4.823×10^{-3}

Table 11 continued

Table 11 (*continued*)

Name	RA(J2000)	DEC(J2000)	Dist(Mpc)	B(mag)	K(mag)	OBS_WINDOW(JD)	SCORE
(1)	(2)	(3)	(4)	(5)	(6)	(7)	(8)
NGC1337	52.03	-8.39	11.91	-18.86	-21.16	2457980.28-2457982.25	4.248×10^{-3}
NGC0988	38.87	-9.36	17.30	-18.98	-24.19	2457980.28-2457982.25	3.882×10^{-3}

Table 12. Galaxies observed after trigger GRB170817a. Table columns provide the galaxy name, coordinates, distance, B and K-band magnitude and the observing window. For the GRB trigger, we selected the 31 most luminous galaxies in the 90% Fermi region (Valenti et al. 2017).

Name	RA(J2000)	DEC(J2000)	Dist(Mpc)	B(mag)	K(mag)	OBS_WINDOW(JD)
(1)	(2)	(3)	(4)	(5)	(6)	(7)
NGC3749	173.97	-38.00	38.02	-20.80	-24.20	2457980.28-2457982.25
NGC3269	157.49	-35.22	36.40	-20.86	-23.75	2457980.28-2457982.25
NGC3273	157.62	-35.61	36.98	-18.99	-23.91	2457980.28-2457982.25
NGC3281C	158.25	-34.89	37.29	-18.79	-22.62	2457980.28-2457982.25
ESO268-003	186.32	-43.45	37.92	-18.95	-23.22	2457980.28-2457982.25
ESO443-042	195.87	-29.83	33.42	-19.69	-22.94	2457980.28-2457982.25
ESO440-004	176.42	-28.37	22.93	-18.82	-18.47	2457980.28-2457982.25
IC4180	196.74	-23.92	33.65	-19.98	-23.04	2457980.28-2457982.25
ESO508-015	197.33	-24.38	33.42	-18.77	-18.79	2457980.28-2457982.25
NGC4806	194.05	-29.50	28.84	-19.26	-21.96	2457980.28-2457982.25
NGC3717	172.88	-30.31	16.90	-19.94	-23.62	2457980.28-2457982.25
NGC3585	168.32	-26.75	20.05	-20.77	-24.81	2457980.28-2457982.25
NGC5365A	209.16	-44.01	36.98	-20.27	-24.00	2457980.28-2457982.25
ESO507-008	191.42	-26.63	33.19	-19.67	-20.51	2457980.28-2457982.25
NGC5161	202.31	-33.17	18.53	-19.84	-22.71	2457980.28-2457982.25
NGC5042	198.88	-23.98	12.65	-18.70	-21.11	2457980.28-2457982.25
ESO572-049	180.85	-19.52	31.62	-18.57	-19.95	2457980.28-2457982.25
ESO126-025	144.64	-61.74	34.42	-19.89	-23.34	2457980.28-2457982.25
NGC4856	194.84	-15.04	11.54	-18.95	-22.84	2457980.28-2457982.25
ESO576-003	197.65	-21.75	28.44	-18.94	-20.65	2457980.28-2457982.25
IC2539	151.07	-31.36	30.76	-19.53	-22.39	2457980.28-2457982.25
ESO435-015	149.46	-31.01	32.36	-18.35	-21.04	2457980.28-2457982.25
ESO176-006	224.29	-54.39	38.01	-21.52	-24.43	2457980.28-2457982.25
ESO435-010	149.09	-31.30	33.28	-18.68	-19.91	2457980.28-2457982.25
ESO092-014	152.72	-66.65	23.96	-19.28	-23.28	2457980.28-2457982.25
NGC5119	201.00	-12.28	35.19	-18.98	-23.08	2457980.28-2457982.25
NGC3952	178.42	-4.00	23.12	-19.62	-20.81	2457980.28-2457982.25
NGC5670	218.90	-45.97	36.98	-19.24	-24.23	2457980.28-2457982.25

Table 12 continued

Table 12 (*continued*)

Name	RA(J2000)	DEC(J2000)	Dist(Mpc)	B(mag)	K(mag)	OBS_WINDOW(JD)
(1)	(2)	(3)	(4)	(5)	(6)	(7)
NGC3915	177.23	-4.68	36.06	-18.51	-21.04	2457980.28-2457982.25
NGC4546	188.87	-3.79	14.06	-19.50	-23.35	2457980.28-2457982.25
ESO097-013	213.29	-65.34	4.21	-19.03	-23.14	2457980.28-2457982.25

Table 13. Galaxies observed after trigger GW170817/G298048. Table columns provide the galaxy name, coordinates, distance, B and K-band magnitude, observing window and the score from our ranking algorithm. It's shown that NGC4993, which is the host galaxy of the kilonova AT17fgo, is ranked by our algorithm as the second in the list, see column 'score'. After taking account of the distance distribution from GW estimation, NGC4993 is the highest ranking galaxy, shown as column 'score2'. The galaxy list is ranked with 'score2'.

Name	RA(J2000)	DEC(J2000)	Dist(Mpc)	B(mag)	K(mag)	OBS_WINDOW(JD)	SCORE	SCORE2
(1)	(2)	(3)	(4)	(5)	(6)	(7)	(8)	(9)
NGC4993	197.45	-23.38	39.99	-20.20	-23.42	2457983.41-2457985.17	1.195×10^{-1}	1.615×10^{-1}
IC4197	197.02	-23.80	34.10	-20.24	-23.39	2457983.41-2457985.17	1.346×10^{-1}	1.386×10^{-1}
ESO508-019	197.47	-24.24	38.55	-19.33	-21.16	2457983.41-2457985.17	1.060×10^{-1}	1.311×10^{-1}
NGC4968	196.77	-23.68	33.42	-19.44	-23.14	2457983.41-2457985.17	1.145×10^{-1}	1.103×10^{-1}
ESO508-024	197.69	-23.87	33.42	-19.98	-21.59	2457983.41-2457985.17	9.862×10^{-2}	1.021×10^{-1}
IC4180	196.74	-23.92	33.65	-19.98	-23.04	2457983.41-2457985.17	9.361×10^{-2}	9.230×10^{-2}
ESO508-015	197.33	-24.38	33.42	-18.77	-18.79	2457983.41-2457985.17	8.194×10^{-2}	7.894×10^{-2}
ESO508-004	196.72	-22.84	33.96	-18.33	-18.75	2457983.41-2457985.17	7.466×10^{-2}	7.586×10^{-2}
ESO508-003	196.60	-24.16	33.43	-19.20	-21.23	2457983.41-2457985.17	5.371×10^{-2}	5.180×10^{-2}
ESO575-053	196.27	-22.38	30.48	-18.44	-21.31	2457983.41-2457985.17	2.850×10^{-2}	1.897×10^{-2}
IC0874	199.75	-27.63	29.06	-19.29	-22.64	2457983.41-2457985.17	1.873×10^{-2}	9.936×10^{-3}
ESO576-001	197.60	-21.68	35.47	-19.18	-22.00	2457983.41-2457985.17	7.000×10^{-3}	8.057×10^{-3}
NGC5078	199.96	-27.41	27.67	-21.24	-25.09	2457983.41-2457985.17	1.685×10^{-2}	6.943×10^{-3}
NGC5061	199.52	-26.84	24.21	-20.82	-24.63	2457983.41-2457985.17	1.935×10^{-2}	3.727×10^{-3}
ESO576-003	197.65	-21.75	28.44	-18.94	-20.65	2457983.41-2457985.17	6.816×10^{-3}	3.242×10^{-3}
ESO508-051	200.12	-26.08	34.04	-18.41	-19.55	2457983.41-2457985.17	1.878×10^{-3}	1.922×10^{-3}
NGC5101	200.44	-27.43	24.21	-20.68	-24.76	2457983.41-2457985.17	6.919×10^{-3}	1.333×10^{-3}
NGC4680	191.73	-11.64	29.92	-19.12	-22.61	2457983.41-2457985.17	1.299×10^{-3}	7.933×10^{-4}
ESO576-005	197.83	-19.83	38.54	-19.04	-20.21	2457983.41-2457985.17	4.122×10^{-3}	3.943×10^{-4}
NGC4663	191.20	-10.20	30.40	-18.75	-22.71	2457983.41-2457985.17	5.385×10^{-3}	3.534×10^{-4}

Table 14. Galaxies observed after trigger G299232. Table columns provide the galaxy name, coordinates, distance, B and K-band magnitude, observing window and the score from our ranking algorithm. The cumulative score is 0.775.

Name (1)	RA(J2000) (2)	DEC(J2000) (3)	Dist(Mpc) (4)	B(mag) (5)	K(mag) (6)	OBS_WINDOW(JD) (7)	SCORE (8)
NGC0772	29.83	19.01	32.36	-21.78	-25.35	2457991.48-2458005.21	5.598×10^{-2}
NGC0524	21.20	9.54	23.99	-20.53	-24.74	2457991.48-2458005.21	5.373×10^{-2}
NGC0770	29.81	18.95	32.36	-18.75	-22.27	2457991.48-2458005.21	5.272×10^{-2}
NGC0518	21.07	9.33	30.31	-19.35	-22.61	2457991.48-2458005.21	5.084×10^{-2}
NGC0525	21.22	9.70	22.32	-18.32	-21.14	2457991.48-2458005.21	5.020×10^{-2}
NGC0516	21.03	9.55	29.87	-18.82	-21.86	2457991.48-2458005.21	4.811×10^{-2}
NGC0532	21.32	9.26	29.92	-19.73	-23.55	2457991.48-2458005.21	4.614×10^{-2}
IC0101	21.04	9.93	30.71	-18.40	-20.56	2457991.48-2458005.21	4.544×10^{-2}
NGC0522	21.19	9.99	29.92	-19.23	-22.94	2457991.48-2458005.21	4.246×10^{-2}
NGC0502	20.73	9.05	30.67	-19.27	-22.70	2457991.48-2458005.21	4.122×10^{-2}
NGC0489	20.47	9.21	29.92	-20.12	-22.82	2457991.48-2458005.21	3.494×10^{-2}
NGC0488	20.45	5.26	29.92	-21.41	-25.42	2457991.48-2458005.21	2.466×10^{-2}
NGC6925	308.59	-31.98	28.31	-21.07	-24.27	2457991.48-2458005.21	2.074×10^{-2}
NGC0628	24.17	15.78	7.31	-19.53	-22.47	2457991.48-2458005.21	1.475×10^{-2}
IC1711	22.73	17.19	35.81	-19.20	-23.23	2457991.48-2458005.21	1.345×10^{-2}
ESO340-012	304.64	-39.34	33.42	-19.15	-21.25	2457991.48-2458005.21	1.189×10^{-2}
UGC01020	21.68	17.26	30.71	-19.02	-21.32	2457991.48-2458005.21	1.182×10^{-2}
ESO340-017	304.92	-39.29	34.44	-20.14	-21.75	2457991.48-2458005.21	1.125×10^{-2}
NGC0474	20.03	3.42	29.92	-20.44	-23.82	2457991.48-2458005.21	1.107×10^{-2}
UGC00958	21.14	16.54	28.87	-18.81	-18.31	2457991.48-2458005.21	1.047×10^{-2}
NGC0520	21.14	3.79	29.92	-20.39	-24.01	2457991.48-2458005.21	1.002×10^{-2}
NGC0470	19.94	3.41	36.14	-20.42	-23.95	2457991.48-2458005.21	9.803×10^{-3}
NGC0514	21.02	12.92	23.99	-19.59	-22.76	2457991.48-2458005.21	9.406×10^{-3}
ESO340-009	304.34	-38.67	29.65	-18.71	-19.96	2457991.48-2458005.21	9.200×10^{-3}
NGC0473	19.98	16.54	29.92	-19.78	-22.82	2457991.48-2458005.21	9.118×10^{-3}
UGC01197	25.64	18.31	35.16	-18.53	-19.97	2457991.48-2458005.21	8.382×10^{-3}
IC5013	307.14	-36.03	29.92	-19.99	-23.77	2457991.48-2458005.21	5.874×10^{-3}
NGC0660	25.76	13.64	9.25	-19.04	-22.49	2457991.48-2458005.21	5.767×10^{-3}
ESO399-025	303.37	-37.19	33.40	-19.29	-22.62	2457991.48-2458005.21	5.604×10^{-3}
ESO400-026	307.04	-35.81	31.71	-18.55	-19.15	2457991.48-2458005.21	5.589×10^{-3}
UGC00903	20.45	17.59	29.92	-18.74	-22.96	2457991.48-2458005.21	5.541×10^{-3}
NGC0485	20.36	7.02	29.92	-18.99	-21.56	2457991.48-2458005.21	4.800×10^{-3}
UGC01110	23.32	13.33	33.73	-18.51	-20.54	2457991.48-2458005.21	4.575×10^{-3}
UGC00964	21.15	7.72	37.84	-18.45	-20.98	2457991.48-2458005.21	4.571×10^{-3}
NGC6923	307.91	-30.83	37.15	-20.51	-24.04	2457991.48-2458005.21	4.456×10^{-3}
ESO340-008	304.30	-40.92	33.42	-19.15	-20.75	2457991.48-2458005.21	4.073×10^{-3}
ESO462-031	307.97	-30.80	33.92	-18.62	-21.43	2457991.48-2458005.21	4.012×10^{-3}
PGC004612	19.18	16.40	28.90	-18.37	-21.15	2457991.48-2458005.21	3.910×10^{-3}

Table 14 continued

Table 14 (*continued*)

Name (1)	RA(J2000) (2)	DEC(J2000) (3)	Dist(Mpc) (4)	B(mag) (5)	K(mag) (6)	OBS_WINDOW(JD) (7)	SCORE (8)
PGC058798	250.51	-5.03	19.95	-19.07	-22.34	2457991.48-2458005.21	3.082×10^{-3}
NGC6106	244.70	7.41	24.66	-19.60	-22.34	2457991.48-2458005.21	3.047×10^{-3}
ESO340-032	306.73	-39.62	33.54	-18.98	-21.17	2457991.48-2458005.21	1.958×10^{-3}